A Semi-Analytical Method for the Calculation of the Elastic Micro-Fields in Plain Weave Fabric Composites Subjected to In-Plane Loading

J. L. KUHN, S. I. HAAN AND P. G. CHARALAMBIDES
Department of Mechanical Engineering
The University of Maryland, Baltimore County
1000 Hilltop Circle
Baltimore, MD 21250

(Received September 5, 1997)
(Revised August 4, 1998)

ABSTRACT: In this paper, a computationally efficient semi-analytical method is developed for the calculation of the elastic micro-fields dominating plain weave composites under remote in-plane loading. The framework needed to obtain analytical displacement estimates is derived using the Rayleigh-Ritz method for a composite plate with spatially varying laminate stiffnesses. The method is developed with the aid of a symmetric woven unit-cell geometry. Three separate boundary value problems, corresponding to remotely applied biaxial and uniaxial displacement, and simple shear boundary conditions are formulated. Unit-cell geometry and material characteristics for both polymer and ceramic matrix composites are incorporated in the formulation of the above boundary value problems.

Extensive solution convergence studies are presented. As expected, convergence is shown to depend on the number of terms used in the Ritz series solution and the number of integration stations used to integrate the spatially laminate stiffnesses within the woven unit-cell geometry. Convergence results for the optimal selection of both of the above parameters are presented. The implications of the method's potential to yield accurate elastic microfields on the evolution of stress induced microdamage in woven systems is discussed.

1. INTRODUCTION

WHILE WOVEN FABRIC composites are considered as an attractive material alternative for many design problems, their mechanical response is not well understood, primarily due to the highly complex nature of the composite morphol-

0021-9983/99/03 0221–46 $10.00/0

ogy. In order to develop reliable predictive mechanics tools that capture in a more realistic manner the non-linear response of such systems, one may need to develop mechanical models that are encompassing of several levels of analysis as needed to account for multiple length scales inherent in these systems. Most attempts at modeling the mechanical response to date have been based on idealized analytical approaches via approximate engineering assumptions [1–11]. Numerous finite element models have been developed and compared to the idealized analytical models [10, 12–14]. A few attempts at more rigorous analytical models have been made but those models ultimately rely on numerical solutions [12–15].

Much work has been done to model the linear behavior of woven polymer matrix composites (PMCs) which by comparison to chemical vapor infiltrated (CVI) ceramic matrix composites (CMCs) exhibit a more regular but yet complex microstructure. Ishikawa and Chou [1–5,16–19] developed analytical models using the classical laminate theory [20] for infinitesimal columns within a simplified 1-D woven unit-cell. Ishikawa et al. [21] reported experimental studies in conjunction with the Ishikawa and Chou [1–5,16–19] models. Naik and Shembekar [6] presented a model based on the classical laminate theory, with a geometry model based on that of Chou and Ishikawa [5], and addressed the 2-D architecture of the woven structure. The latter models were improved by Naik and Shembekar [6] to account for 2-D geometry effects. In their studies, Naik and Shembekar also presented improved methods of property averaging, and took into account the microstructure of the tows using the Composite Cylinder Assemblage (CCA) model of Hashin [22]. Raju and Wang [9] presented models similar to that of Naik and Shembekar for plain weave, five-, and eight-harness satin weave composites, using a more approximate approach to property averaging and without taking into account the microstructure of the tows. R. A. Naik [16,18] presented a general purpose micromechanics models for woven and braided fabric reinforced composites. A Repeating Unit Cell (RUC) modeling approach was applied to model the three-dimensional geometry of plain and satin weave as well as 2-D braided and 2-D triaxial braided composites. The above geometry models were developed based on simplifying assumptions regarding the yarn cross-sectional shapes. In addition, the effective property estimates were obtained using assumptions of iso-strain distribution over the length of the unit-cell. While such assumptions may yield good estimates of the effective properties of the composite, the same assumptions lead to severe discrepancies when predicting the associated elastic micro-fields (see References [23,24]).

In all of the above models, the effective properties are computed by assuming that either the local strains or the resultant forces are constant. For the constant strain or iso-strain assumption (the "parallel" P-MLT model used in References [23] and [24]) the average resultant forces are computed to yield the effective properties. If the resultant forces are assumed constant (the "series" S-MLT model reported in [23]), then the converse is pursued. Naik and Shembekar [6] improved

on these assumptions by assuming that the strains are constant in one direction, and the resultant forces are constant in the other (the "parallel-series" PS-MLT model in Reference [23]), as well as the converse of this combination (the "series-parallel" SP-MLT model in Reference [23]). The results of Whitcomb [13] illustrate that under uniaxial tension the micro-strains are complex and the above assumptions are not locally accurate. While these approximations are accurate in the global sense, and hence do yield good estimates for the effective elastic properties [23,24], they represent gross approximations when estimating the micro-stress fields in such complex woven systems.

The above analytical approaches are based on the classical laminate theory and, as such, yield engineering approximations of the effective properties. Shkoller and Hegemier [15] and Dasgupta and Bhandarkar [14] performed rigorous mathematical homogenization of the unit-cell. Due to the complex geometry of the woven unit-cell, both Shkoller and Hegemier [15] and Dasgupta and Bhandarkar [14] obtained the effective properties of the woven unit-cell via the finite element method. While the accuracy of these studies yield improved results for the effective mechanical response of the woven system, they are somewhat impractical for design applications. Zhang and Harding [12] used an energy equivalence method and finite element analysis to determine the approximate effective properties of a one-dimensional undulation model, much like the fiber undulation model of Ishikawa and Chou [4]. Whitcomb [13] presented a three-dimensional finite element model to determine the micro-stresses and effective elastic properties of a plain weave composite. Whitcomb also used an energy equivalence method in conjunction with the use of an average stress and strain in determining the effective woven unit-cell properties. In addition to providing estimates for the effective elastic properties, the finite element method solves the three-dimensional elasticity boundary value problem. As such, the method yields the micro-field quantities required for damage assessment. Dasgupta and Bhandarkar [14] utilized the local strain results to model the non-linear "knee" behavior observed in woven PMCs. These studies indicated that the determination of the local micro-stresses in complex woven systems depends critically on our ability to predict accurately the spatially varying mid-plane deformations, strains, and curvatures of the woven laminate. Accurate micro-stress estimates are needed for the evaluation of stress induced microdamage that is often observed in both polymer and ceramic matrix woven systems.

As mentioned previously, the assumptions of uniform strain and/or uniform resultant forces used to predict the effective elastic response are not sufficient to accurately predict local micro-stresses and thus microdamage in the woven unit-cell. Naik and Ganesh [11] employed the method of cells [25] to improve the micro-strain estimates. The method involves simplifying the geometry into rectangular blocks called sub-cells, and enforcing displacement and traction continuity along the interfaces of the sub-cells in an average sense. While this method appears to

yield reasonable estimates for the micro-strains, the analysis is relatively involved, and the effects of simplifying the geometry in this fashion are unknown. In addition Naik and Ganesh assumed that local warping due to the unbalanced stacking within the unit-cell is suppressed. This assumption may have significant limitations, particularly in the case of polymer matrix composites. Cox in Reference [17] presents a review of several failure models for textile composites. In Reference [19], Cox and Flanagan present a rather extensive summary of existing models for textile composites while also reviewing the various implementation codes of some of the analysis models.

In this work, it is recognized that the woven unit-cell biaxial loading and simple shear boundary value problems may be formulated as a composite plate elasticity problem by employing the Kirchhoff-Love deformation hypothesis, and by allowing the composite stiffnesses to vary with position. The resulting governing differential equations are similar to those presented in References [20,26] with the exception that the coefficients of the equilibrium partial differential equations vary spatially. As such, an exact solution of the woven plate elasticity boundary value problem may not be readily obtained. However, because the domain geometry and boundary conditions of the problem can readily be posed mathematically, the elasticity solution may be approximated using the Rayleigh-Ritz method [27]. An approximate analytical solution of this form would offer improved micro-strain estimates when compared to those obtained using the modified lamination theory and the method of cells. At the same time, it is expected that such solutions can be obtained at a fraction of the computational cost needed for detailed 3-D finite element analysis. Finally, the solution would indeed be simpler than the method of cells which involves a rather demanding subdivision process. Several researchers have employed the Rayleigh-Ritz method of approximation in the analysis of composite plates [28–30], however, emphasis has been placed on the bending response of laminates of constant layer thickness. The analysis of laminated plates comprised of layers with spatially varying thicknesses, such as the plain weave composite system, has not yet been undertaken.

A great deal of work has been done to develop improved theories over those of the Kirchhoff-Love deformation hypothesis [31–41] for composites with thick sections and other configurations where the deformation through the depth of the composite does not remain linear. Due to the highly irregular woven morphology, these effects may also be important in woven fabric composites. However, an approximate solution of the elasticity equations in conjunction with the Kirchhoff-Love assumptions represents an improvement over the current methods of woven composite analysis, and is a critical first step worth investigating prior to pursuing other higher order theories.

The accurate analysis of woven composite linear response forms the critical basis for further investigations on the stress induced microdamage evolution, R-curve behavior, and ultimate failure of this complex class of material systems.

Simple, convenient, and accurate means of obtaining the linear elastic micro-fields are required because the linear analysis phase represents one step in an otherwise lengthy iterative procedure employed in the determination of the effective non-linear response of the systems under consideration.

2. BOUNDARY VALUE PROBLEM FORMULATION

In an effort to understand the in-plane response of plain weave fabric composites, three separate boundary value problems are considered. In each case, the solution domain is defined to be the woven unit-cell of height h and tow undulation half period a as shown in Figure 1. The geometry functions for each of the unit-cells shown in Figure 1 are presented in detail in Reference [42]. The symmetry of the unit-cell geometry about each face normal to the x-y plane is used to formulate the appropriate boundary conditions representing an infinite plate with periodic woven morphology as discussed elsewhere [23,24,42].

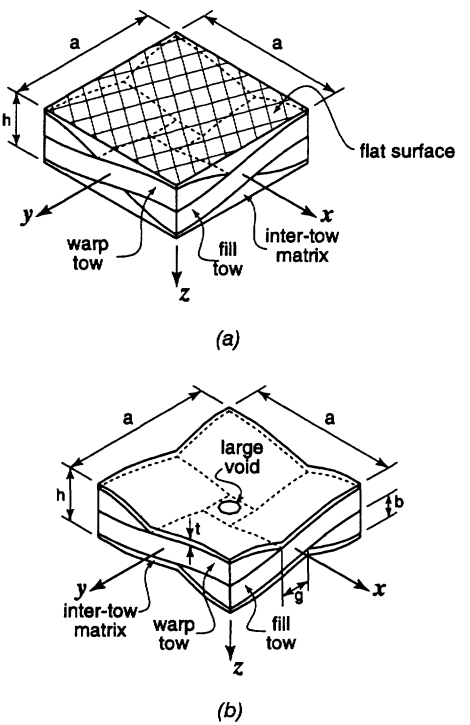

Figure 1. *Plain weave fabric symmetric unit-cells used in the development of the approximate analytical elasticity solutions: (a) the porous matrix geometry model used to simulate soft-polymer matrix composites and (b) the matrix layer geometry model associated with stiff-ceramic matrix plain weave fabric composites.*

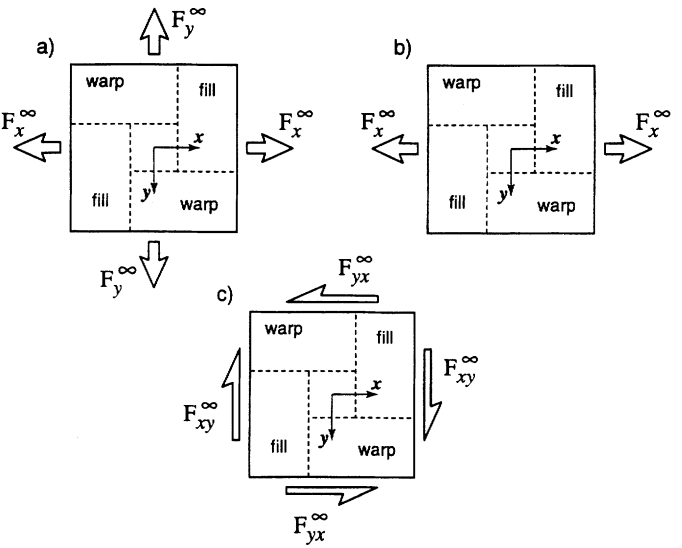

Figure 2. *Top views of a woven unit-cell subjected to: in-plane (a) biaxial tension, (b) uniaxial tension, and (c) simple shear.*

The overall objectives of the analysis are two-fold. First, the micro-strains throughout the unit-cell under remotely applied in-plane loading are to be determined. The second objective is to compute the effective in-plane properties E_x,ν_{xy}, and G_{xy} of the woven composite. Solutions of the biaxial and shear problems shown in Figures 2(a) and 2(c), respectively, will be pursued as part of the first objective. For the second objective, the uniaxial and simple shear problems depicted in Figures 2(b) and 2(c) will be considered as required to compute the requisite effective in-plane properties. In Figure 2 the remotely applied loads are represented with the forces F_x^∞, F_y^∞ and $F_{xy}^\infty = F_{yx}^\infty$. For the purpose of this analysis, these remotely applied loads must be specified as either traction or displacement boundary conditions along the edges of the unit-cell. In this study, due to geometric, loading, and material symmetry, we shall employ readily enforceable displacement boundary conditions. Hence, the terminology biaxial or uniaxial displacement, and simple shear conditions will be used to refer to the three problems with displacement boundary conditions corresponding to the configurations shown in Figure 2.

The overall height h to undulation half period a ratio for plain weave fabric composites are generally small. As such, the woven fabric composite may be classified as a non-uniform laminated plate. A brief review of the governing elasticity equations for a plain weave fabric composite plate are presented in the next section. In subsequent sections, the geometry of the unit-cell is better defined and the principle of virtual work and the specific boundary conditions are employed for the three problems under consideration.

2.1 Non-Uniform Laminated Plate Theory

A global coordinate system with its origin and its x and y axes located in the mid-plane of the plate is adopted as the global reference system. The out-of-plane stresses in the plate are neglected, thus giving rise to plane stress conditions. In plain weave fabric composites, the principle material axes of the orthotropic tows undulate out of the plane about the global x and y coordinate axes as discussed elsewhere [42]. At the same time, the tows are not rotated about the z axis normal to the plane of the plate. As a result, the local stiffness coupling terms remain zero and the local stress-stain relations are reduced to

$$\begin{Bmatrix} \sigma_x \\ \sigma_y \\ \tau_{xy} \end{Bmatrix} = \begin{bmatrix} \overline{Q}_{11} & \overline{Q}_{12} & 0 \\ \overline{Q}_{12} & \overline{Q}_{22} & 0 \\ 0 & 0 & \overline{Q}_{66} \end{bmatrix} \begin{Bmatrix} \varepsilon_x \\ \varepsilon_y \\ \gamma_{xy} \end{Bmatrix} \tag{1}$$

The stiffness terms $\overline{Q}_{ij}$, with $i = 1, 2, 6$, may be computed by an appropriate coordinate transformation under the assumption of plane stress as given in References [23,43]. In the classical lamination theory (see Reference [20]), the overbar stiffness notation used above is used to represent the stiffnesses for a generally orthotropic system which accounts for in-plane off-axis loading. With that in mind, it is stressed that the overbar stiffness used in Equation (1) above, are different from those obtained for a generally orthotropic material, for, they are derived consistent with an out-of-plane rotation as needed to account for the out-of-plane orientation of the undulating woven bundles.

The thickness of the woven plate is generally small relative to the in-plane dimensions. The small aspect ratio allows for application of the Kirchhoff-Love assumption that straight lines normal to the undeformed mid-plane remain straight and normal to the deformed mid-plane after loading and the strains along a line normal to the mid-plane are related to the mid-plane strains as follows

$$\begin{Bmatrix} \varepsilon_x \\ \varepsilon_y \\ \gamma_{xy} \end{Bmatrix} = \begin{Bmatrix} \varepsilon_x^0 \\ \varepsilon_y^0 \\ \gamma_{xy}^0 \end{Bmatrix} + z \begin{Bmatrix} \kappa_x^0 \\ \kappa_y^0 \\ \kappa_{xy}^0 \end{Bmatrix} \tag{2}$$

where the components of the above vectors are the strains and curvatures at the mid-plane and are defined as

$$\begin{aligned} \varepsilon_x^0 &= u_{0,x} & \kappa_x^0 &= -w_{0,xx} \\ \varepsilon_y^0 &= v_{0,y} & \kappa_y^0 &= -w_{0,yy} \\ \gamma_{xy}^0 &= u_{0,y} + v_{0,x} & \kappa_{xy}^0 &= -2w_{0,xy} \end{aligned} \tag{3}$$

The "0" subscript indicates the respective field quantity is at the mid-plane of the composite plate, and the comma notation is used to denote the partial derivative with respect to the trailing variable. Thus, the notation $w_{0,x}$ denotes the partial derivative of the mid-plane displacement in the z direction, with respect to x.

From Equations (1) and (2), the local stresses at a point in the plate are written in terms of the mid-plane strains and curvatures as

$$\begin{Bmatrix}\sigma_x\\ \sigma_y\\ \tau_{xy}\end{Bmatrix}=\begin{bmatrix}\overline{Q}_{11} & \overline{Q}_{12} & 0\\ \overline{Q}_{12} & \overline{Q}_{22} & 0\\ 0 & 0 & \overline{Q}_{66}\end{bmatrix}\begin{Bmatrix}\varepsilon_x^0\\ \varepsilon_y^0\\ \gamma_{xy}^0\end{Bmatrix}+z\begin{bmatrix}\overline{Q}_{11} & \overline{Q}_{12} & 0\\ \overline{Q}_{12} & \overline{Q}_{22} & 0\\ 0 & 0 & \overline{Q}_{66}\end{bmatrix}\begin{Bmatrix}\kappa_x^0\\ \kappa_y^0\\ \kappa_{xy}^0\end{Bmatrix} \tag{4}$$

where the mid-plane strains ε_i^0 and curvatures κ_i^0, with $i = 1,2,3$ representing the x, y, and xy components, are continuously varying functions of x and y. The stiffness terms $\overline{Q}_{ij}$ are also functions of x and y, and may be different for each layer in the plate, resulting in a discontinuous z variation of the $\overline{Q}_{ij}$ terms. The work conjugate resultant forces N_i and moments M_i, with $i = 1,2,3$ representing the x, y, and xy components, are computed by integrating the stresses through the depth of the plate and are given by

$$\begin{Bmatrix}N_x\\ N_y\\ N_{xy}\end{Bmatrix}=\int_{s^b(x,y)}^{s^t(x,y)}\begin{Bmatrix}\sigma_x\\ \sigma_y\\ \tau_{xy}\end{Bmatrix}dz$$

$$\begin{Bmatrix}M_x\\ M_y\\ M_{xy}\end{Bmatrix}=\int_{s^b(x,y)}^{s^t(x,y)}\begin{Bmatrix}\sigma_x\\ \sigma_y\\ \tau_{xy}\end{Bmatrix}z\,dz \tag{5}$$

where the functions $s^t(x,y)$ and $s^b(x,y)$ represent the distance from the composite mid-plane to the composite top and bottom surfaces, respectively. In general, these may be functions of x and y for a plate with non-uniform thickness. The local woven composite laminate constitutive relations are computed by substituting Equation (4) into Equation (5) resulting in

$$\begin{Bmatrix}N_x\\ N_y\\ N_{xy}\\ M_x\\ M_y\\ M_{xy}\end{Bmatrix}(x,y)=\begin{bmatrix}A_{11} & A_{12} & 0 & B_{11} & B_{12} & 0\\ A_{12} & A_{22} & 0 & B_{22} & B_{22} & 0\\ 0 & 0 & A_{66} & 0 & 0 & B_{66}\\ B_{11} & B_{12} & 0 & D_{11} & D_{12} & 0\\ B_{12} & B_{22} & 0 & D_{12} & D_{22} & 0\\ 0 & 0 & B_{66} & 0 & 0 & D_{66}\end{bmatrix}(x,y)\begin{Bmatrix}\varepsilon_x^0\\ \varepsilon_y^0\\ \gamma_{xy}^0\\ \kappa_x^0\\ \kappa_y^0\\ \kappa_{xy}^0\end{Bmatrix}(x,y) \tag{6}$$

where the spatially varying local stiffness terms for a fabric composite which may be reduced to the four layers labeled in Figure 3, are computed as follows:

$$A_{ij} = [s^t_{lm} - s^b_{lm}]\overline{Q}^{lm}_{ij} + [s^t_f - s^b_f]\overline{Q}^{f}_{ij} + [s^t_w - s^b_w]\overline{Q}^{w}_{ij} + [s^t_{um} - s^b_{um}]\overline{Q}^{um}_{ij}$$

$$B_{ij} = \frac{1}{2}\{[(s^t_{lm})^2 - (s^b_{lm})^2]\overline{Q}^{lm}_{ij} + [(s^t_f)^2 - (s^b_f)^2]\overline{Q}^{f}_{ij}$$

$$+ [(s^t_w)^2 - (s^b_w)^2]\overline{Q}^{w}_{ij} + [(s^t_{um})^2 - (s^b_{um})^2]\overline{Q}^{um}_{ij}\} \tag{7}$$

$$D_{ij} = \frac{1}{3}\{[(s^t_{lm})^3 - (s^b_{lm})^3]\overline{Q}^{lm}_{ij} + [(s^t_f)^3 - (s^b_f)^3]\overline{Q}^{f}_{ij}$$

$$+ [(s^t_w)^3 - (s^b_w)^3]\overline{Q}^{w}_{ij} + [(s^t_{um})^3 - (s^b_{um})^3]\overline{Q}^{um}_{ij}\}$$

In the above equations the script notation *lm* and *um* denotes the lower and upper matrix layers, respectively, as shown in Figure 3. Likewise, the superscripts *w* and *f* denote the warp and fill tow layers, respectively. While the local stiffnesses $\overline{Q}^{k}_{ij}$ with $k = lm, w, f, um$, remain functions of x and y, and may be different for different layers, they are assumed constant through the thickness of each layer in the above expressions. For example, the local stiffnesses of the warp tows $\overline{Q}^{w}_{ij}$ vary in x due to the tow undulation, and differ from those of the fill tows due to the relative 90° rotation of the principle material axes about the z axis. For non-hybrid woven composites, the local stiffnesses of the warp and fill tows, $\overline{Q}^{w}_{ij}$ and $\overline{Q}^{f}_{ij}$, are computed with an appropriate coordinate transformation from the transversely isotropic effective tow properties, E_1, E_2, G_{12}, ν_{12}, and ν_{23}, where E_1 and E_2 are the longitudinal and transverse moduli respectively, G_{12} is the in-plane shear modulus, and ν_{12} and ν_{23} are the major Poisson's ratios. Above, the subscript 1 denotes the principal material direction aligned with the fiber direction in the tow, and the subscripts 2 and 3 denote the mutually orthogonal transverse principal material directions. For a transversely isotropic material, the transverse shear modulus is related to the above properties by

$$G_{23} = \frac{E_2}{2(1+\nu_{23})} \tag{8}$$

and the remaining orthotropic properties are

$$E_3 = E_2 \qquad \nu_{13} = \nu_{12} \qquad G_{13} = G_{12} \tag{9}$$

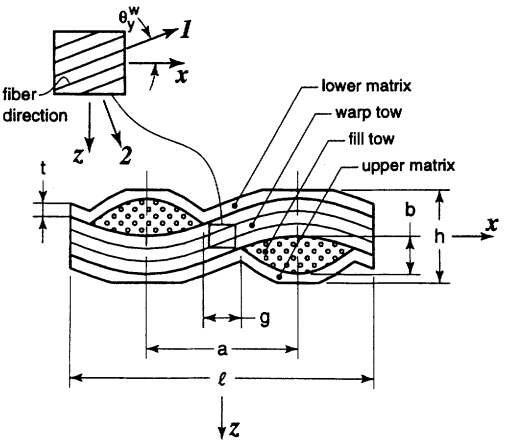

Figure 3. *Woven unit-cell cross-sectional geometry. For these studies the unit-cell length* l *is set equal to the unit-cell undulation half-period* a.

The local stiffnesses of the upper and lower matrix layers, $\overline{Q}_{ij}^{um}$ and $\overline{Q}_{ij}^{lm}$, are computed using the isotropic effective matrix properties $E_{\overline{m}}$ and $\nu_{\overline{m}}$. The effective tow and matrix properties discussed above, may be computed for microstructures typical of polymer and ceramic matrix composites via the micromechanics modeling presented in Reference [23]. In addition, the transformed local stiffnesses $\overline{Q}_{ij}^{w}$ and $\overline{Q}_{ij}^{f}$ are calculated as discussed above and the local stiffnesses $\overline{Q}_{ij}^{um}$ and $\overline{Q}_{ij}^{lm}$ are computed in terms of $E_{\overline{m}}$ and $\nu_{\overline{m}}$ as discussed in Reference [23].

In Equation (7) the functions s_k^t and s_k^b, with $k = lm, w, f, um$, denote the distance from the composite mid-plane to the respective layer top and bottom surfaces. These surfaces may spatially vary with x and y, as is the case with woven composites, or may be constant as is the case for traditional laminated composites. The mathematical functions describing the top and bottom surfaces of each phase in the woven composite are presented in detail in Reference [42] and may be abbreviated as

$$s_{lm}(\eta, x, y) = \begin{cases} s_{lm}^b(x, y) & \eta = -1 \\ s_{lm}^t(x, y) & \eta = +1 \end{cases} \qquad s_f(\eta, x, y) = \begin{cases} s_f^b(x, y) & \eta = -1 \\ s_f^t(x, y) & \eta = +1 \end{cases}$$

$$s_{um}(\eta, x, y) = \begin{cases} s_{um}^b(x, y) & \eta = -1 \\ s_{um}^t(x, y) & \eta = +1 \end{cases} \qquad s_w(\eta, x, y) = \begin{cases} s_w^b(x, y) & \eta = -1 \\ s_w^t(x, y) & \eta = +1 \end{cases} \tag{10}$$

where the parameter $\eta = +1$ corresponds with the top surface and $\eta = -1$ represents the bottom surface.

The above formulation is not restricted to plain weave fabric composites. The laminate stiffnesses given by Equation (7) are the local laminate stiffnesses at each point in the domain of the non-uniform composite plate. This single set of expressions apply throughout the domain and are general in the sense that they describe the stiffnesses of all woven architectures which can be reduced to a four layer non-uniform laminated plate. When four layers are not sufficient to describe the woven morphology, additional layers may be included as needed to take into account tows woven in arbitrary directions in the plane of the composite plate. The approach may even have potential application to three-dimensional braided composites as long as the assumptions of plane stress and Kirchhoff-Love are at least approximately satisfied. As mentioned earlier in this section, a detailed description of the adopted unit-cell geometry is presented elsewhere [42].

In the next section, the functions used to define the plain weave fabric morphology for typical polymer matrix and ceramic matrix composites developed in [42] are presented for completeness.

2.2 Plain Weave Fabric Unit-Cell Geometry

The structure of the woven unit-cell is inherently complex due to the interlacing of bundles of fibers, called tows, and various methods of introducing the matrix material. In describing the geometry, the unit-cell is considered as a three phase system. Two of the phases are the warp and fill tows, and the third is the matrix between tows called inter-tow matrix. Each of these meso-scopic phases are in turn comprised of complex microstructural features such as the fibers, the matrix, and fiber and/or bundle coatings, as well as dispersed porosity within the matrix phases. Modeling of the woven unit-cell response consists of computing effective properties of the tows and inter-tow matrix, and subsequently formulating problems in terms of the three effective phases. The example of a woven composite cross section in Figure 3 illustrates the key geometrical features and parameters of the three phases that together form the plain weave architecture.

The most common woven composites are constructed from brittle continuous bundles of fibers embedded in a polymer matrix, and may take the form of several different architectures, one of which is the plain weave shown in Figure 1. In *soft*-polymer matrix woven composites, the inter-tow matrix fully occupies the space outside the tows as shown in Figure 1(a), and at the same time may contain dispersed micro-porosity. In addition to polymer matrix woven fabric composites, new technologies have enabled the fabrication of woven ceramic matrix systems via the CVI technique. *Stiff*-ceramic matrix woven composites differ from *soft*-polymer matrix composites not only in the properties of the constituent materials, but also in the geometrical form of the inter-tow matrix. The CVI process results in large scale matrix voids and as a result the inter-tow matrix material appears as a layer of relatively uniform thickness that conforms to the shape of

the underlying tows as shown in Figures 1(b) and 3. At the center of the unit-cell, the large scale voids join to form a through hole, which plays a critical role in the distribution of micro-strains.

The composite stiffness formulation summarized in the previous section is applicable to both of the above unit-cell architectures. The focus of this study is placed on *soft*-polymer and *stiff*-ceramic matrix woven systems. As such, the geometry models characteristic of each system are briefly outlined in this section. While other researchers have developed various geometric models for plain weave systems (see for example References [16,19]), a detailed discussion of the plain weave geometry and surface function formulation used for this study is presented in Reference [42].

While the microstructure of polymer and ceramic matrix composite tows differ significantly, the effective tow structures are virtually identical. The functions of Equation (10) which describe the top and bottom surfaces for plain weave fabric composite tows may be written as

$$\begin{aligned} s_w(\eta, x, y) &= s_{tow}(\eta, x, y) \qquad \text{(warp tow)} \\ s_f(\eta, x, y) &= -s_{tow}(-\eta, y, x) \qquad \text{(fill tow)} \end{aligned} \tag{11}$$

where the function s_{tow} can be found in References [42,44]. The surface functions of the inter-tow matrix in the porous matrix model used to simulate the geometry of *soft*-polymer matrix composites are

$$\begin{aligned} s_{lm}(\eta, x, y) &= \begin{cases} -\dfrac{h}{2} & \eta = -1 \\ s_m(-1, x, y) & \eta = +1 \end{cases} \qquad \text{(lower matrix)} \\ s_{um}(\eta, x, y) &= \begin{cases} s_m(+1, x, y) & \eta = -1 \\ +\dfrac{h}{2} & \eta = +1 \end{cases} \qquad \text{(upper matrix)} \end{aligned} \tag{12}$$

where h is the overall height of the composite plate and the general matrix function $s_m(\eta, x, y)$ can also be found in References [42,44]. The top and bottom surface functions of the tows in the matrix layer model associated with CVI ceramic matrix composites are also given by Equation (11), and the matrix surface functions are

$$\begin{aligned} s_{lm}(\eta, x, y) &= \begin{cases} \text{MAX}\left(s_m(-1, x, y) - t_m(x, y), -\dfrac{h}{2}\right) & \eta = -1 \\ s_m(-1, x, y) & \eta = +1 \end{cases} \qquad \text{(lower matrix)} \\ s_{um}(\eta, x, y) &= \begin{cases} s_m(+1, x, y) & \eta = -1 \\ \text{MAX}\left(s_m(+1, x, y) + t_m(x, y), +\dfrac{h}{2}\right) & \eta = +1 \end{cases} \qquad \text{(upper matrix)} \end{aligned} \tag{13}$$

where the function $t_m(x, y)$ is given in [42,44]. The above geometry shape functions may be used in conjunction with the tow and matrix effective properties to compute the local composite stiffnesses of Equation (6). These composite stiffnesses are ultimately functions of x and y due to the variation in geometry.

2.3 The Principle of Virtual Work Applied to Woven Composite Plates

The plate elasticity formulation presented in Section 2.1 involves the following 15 unknowns:

$$\begin{array}{llll} u_0 & v_0 & w_0 & \rightarrow \text{mid-plane displacements} \\ \varepsilon_x^0 & \varepsilon_y^0 & \gamma_{xy}^0 & \rightarrow \text{mid-plane strains} \\ \kappa_x^0 & \kappa_{xy}^0 & \kappa_{xy}^0 & \rightarrow \text{mid-plane curvatures} \\ N_x & N_y & N_{xy} & \rightarrow \text{resultant forces} \\ M_x & M_y & M_{xy} & \rightarrow \text{resultant moments} \end{array} \tag{14}$$

Equations (3) and (6) give rise to 12 partial differential equations involving the above 15 unknowns. Thus, the complete definition of the requisite boundary value problem requires an additional set of three equations plus the specification of the related boundary conditions. A sufficient set could be derived via the equations of equilibrium. However, even though the domain of the geometry is mathematically well posed, an exact solution of this set of partial differential equations would be almost intractable, because Equation (6) involves spatially dependent coefficients. Alternatively, one may derive the weak or variational form of the equilibrium equations or write a minimizing principle and employ the Rayleigh-Ritz approximate method of solution. In the theory of elasticity, the weak form of the equilibrium equations is equivalent to the statement of the principle of virtual work, and conversely the equilibrium equations represent the Euler equations which can be derived from the variational statement of the principle of virtual work.

In this section we shall employ the principle of virtual work as needed to derive the governing plate equations in the weak and variational form. We shall then identify the associated essential and natural boundary conditions for the in-plane loading under consideration.

The total potential energy Π of a deformable body is written in terms of the total strain energy U and the potential energy of external forces W as

$$\Pi = U - W \tag{15}$$

As stated by the principle of minimum potential energy, in an elastic system the potential energy assumes a global minimum for the actual displacements induced by the applied loads under the specified kinematic displacement constraints. As

such the first variation of the potential energy under a virtual displacement, δu, should be zero, and thus the variational form of the principle of virtual work is given by:

$$\delta\Pi = \delta U - \delta W = 0 \tag{16}$$

In the absence of body forces, the above equation may be written in terms of the stresses σ_{ij}, strain increments $\delta\varepsilon_{ij}$, tractions t_i and displacement increments δu_i as follows:

$$\delta\Pi = \int_V \sigma_{ij}\,\delta\varepsilon_{ij}\,dV - \oint_S t_i \delta u_i dS = 0 \tag{17}$$

where $i,j = 1,2,3$ represents the x, y, and z directions, and dV and dS are the volume and surface differential elements, respectively, as shown in Figure 4. Consistent with the Kirchhoff-Love deformation hypothesis the virtual displacements δu_i expressed in terms of the mid-plane virtual displacements and their derivatives are:

$$\begin{aligned} \delta u &= \delta u_0 - z\delta w_{0,x} \\ \delta v &= \delta v_0 - z\delta w_{0,x} \\ \delta w &= \delta w_0 \end{aligned} \tag{18}$$

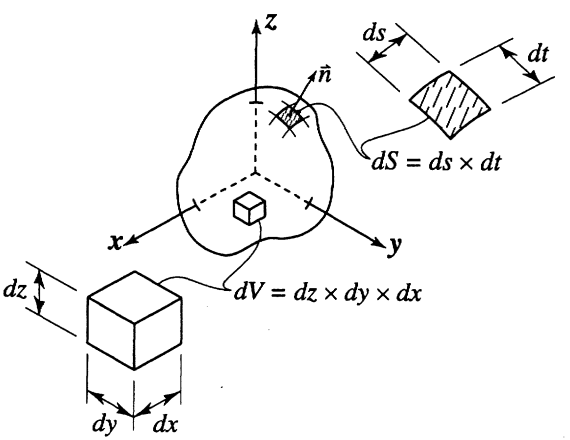

Figure 4. *Volume and surface differential elements of a three-dimensional deformable solid.*

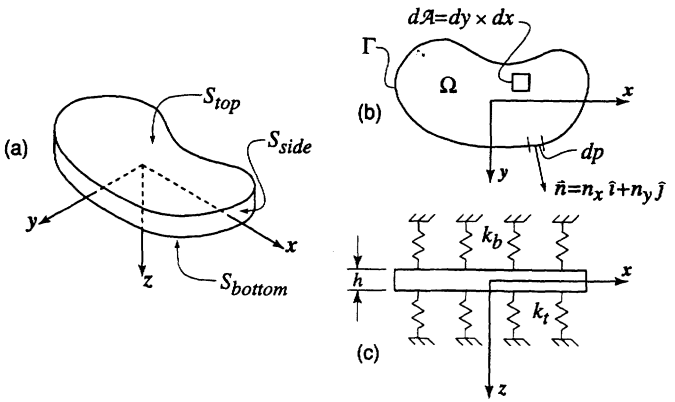

Figure 5. *Characteristics of a thin plate: (a) top, bottom, and side surfaces of the plate; (b) top view of the plate illustrating the domain Ω and boundary differential elements $d\mathcal{A}$ and dp respectively and (c) the top and bottom plate surfaces are constrained by elastic springs of stiffness k_t and k_b respectively.*

and the virtual strains written in terms of the virtual displacements using Equation (3) are

$$\delta\varepsilon_x = \delta u_{0,x} - z\delta w_{0,xx}$$

$$\delta\varepsilon_y = \delta v_{0,x} - z\delta w_{0,yy} \tag{19}$$

$$\delta\gamma_{xy} = \delta u_{0,y} + \delta v_{0,x} - 2z\delta w_{0,xy}$$

The deformable body in Figure 4 represents an arbitrary three-dimensional shape, and as such, may be characterized by three orthonormal length dimensions, i.e., height, width, and depth. If one of these dimensions is small relative to the other two, the body is represented as a plate as shown in Figure 5. Three different views are displayed to demonstrate the key features of a general thin plate. Figure 5(a) illustrates the relationship of the three surfaces which together form the closed boundary surface of the plate. In two dimensions, the plate is comprised of the domain Ω and boundary Γ as shown in Figure 5(b), and the top and bottom elastic foundations with stiffnesses k_t and k_b are shown in the side view of Figure 5(c). These springs can be used to simulate the effects of an elastic foundation such as the presence of adjacent elastically deforming plies in multiple ply composite laminates. Under the assumption of plane stress conditions which may be applied to the plate geometry shown in Figure 5, and with the aid of Equations (4)–(6) as well as Equations (18) and (19), Equation (17) takes the following form:

$$\delta\Pi = \int_{\Omega} \{N_x \delta u_{0,x} + N_{xy}(\delta u_{0,x} + \delta v_{0,x}) + N_y \delta v_{0,y}$$

$$- M_x \delta w_{0,xx} - 2M_{xy} \delta w_{0,xy} + M_y \delta w_{0,yy} + k_m w_0 \delta w_0 \} dA$$

$$- \oint_{\Gamma} \{(N_x n_x + N_{xy} n_y)\delta u_0 + (N_{xy} n_x + N_y n_y)\delta v_0 + (Q_x n_x + Q_y n_y)\delta w_0$$

$$- (M_x n_x + M_{xy} n_y)\delta w_{0,x} - (M_{xy} n_n + M_y n_y)\delta w_{0,y}\} dp + 0 \qquad (20)$$

In the above equation, a cumulative effective elastic foundation stiffness at the mid-plane of the plate $k_m = k_t + k_b$ is employed, where k_m may spatially vary with x and y. In addition, the resultant forces N_i and moments M_i, with $i = x,y,xy$, are defined by Equation (5), and the transverse resultant shear terms Q_x and Q_y are

$$\begin{Bmatrix} Q_x \\ Q_y \end{Bmatrix} = \int_{s^b(x,y)}^{s^t(x,y)} \begin{Bmatrix} \tau_{xz} \\ \tau_{yz} \end{Bmatrix} dz \qquad (21)$$

A detail derivation of the above equation can be found in Reference [44]. As discussed in Reference [44], the above expanded potential energy variational form, is derived with no restrictions placed on the composition of the plate shown in Figure 5 under the Kirchhoff-Love deformation hypothesis assumption. Material heterogeneities combined with the woven distribution of the constituents of a woven composite plate may result in a violation of the above deformation hypothesis. While many researchers have employed this assumption with reasonable success [1,5,6,9,23], care must be taken to observe this limitation for systems with unusual morphology such as the woven composite.

The equilibrium differential equations may be obtained from Equation (20) by integrating by parts, collecting the coefficients of the variational terms, and noting that the expression holds for arbitrary and independent variations in the primary variables u, v, w. From the above virtual statement the essential and natural boundary conditions of the problem are identified as

essential	natural
u_0	$N_x n_x + N_{xy} n_y$
v_0	$N_y n_y + N_{xy} n_x$
w_0	$Q_x n_x + Q_y n_y$
$w_{0,x}$	$M_x n_x + M_{xy} n_y$
$w_{0,y}$	$M_y n_y + M_{xy} n_x$

(22)

where n_x and n_y are the direction cosines of the normal to the boundary Γ. Because the boundary normal is parallel to the xy plane, $n_z = 0$. Equations (3), (6) and (20) in conjunction with the boundary conditions of specific problems are sufficient to solve for the unknowns given in Equation (14). In the next section we shall identify the appropriate boundary conditions for three loading configurations of the plain weave unit-cell shown schematically in Figure 2.

2.4 Boundary Conditions

In order to study general in-plane loading, the two boundary value problems of biaxial and simple shear loading are considered. The problems are formulated in terms of displacement boundary conditions to take advantage of the geometric symmetry along the edges of the woven unit-cell. The boundary conditions employed for the biaxial displacement problem are shown in Figure 6. The four edges of the unit-cell are labeled with Γ_i, where $i = 1 \ldots 4$, to associate the boundary condition with the segment over which it is applied. Here symmetry conditions are applied along the left and bottom edges, labeled Γ_2 and Γ_3, respectively. Uniform displacements u_y^∞ and u_x^∞ are applied along the top and right (Γ_1 and Γ_4) edges respectively. The uniform displacement boundary conditions also simulate symmetry about the respective edge. The detailed boundary conditions of the biaxial displacement problem are as follows:

$$\begin{array}{llll} n_x = 0 & v_0 = u_y^\infty & N_{xy} = 0 & \\ n_y = +1 & w_{0,y} = 0 & M_{xy} = 0 & \text{on } \Gamma_1 \\ & & Q_y = 0 & \end{array} \tag{23}$$

$$\begin{array}{llll} n_x = -1 & u_0 = 0 & N_{xy} = 0 & \\ n_y = 0 & w_{0,x} = 0 & M_{xy} = 0 & \text{on } \Gamma_2 \\ & & Q_x = 0 & \end{array} \tag{24}$$

$$\begin{array}{llll} n_x = 0 & v_0 = 0 & N_{xy} = 0 & \\ n_y = -1 & w_{0,y} = 0 & M_{xy} = 0 & \text{on } \Gamma_3 \\ & & Q_y = 0 & \end{array} \tag{25}$$

$$\begin{array}{llll} n_x = +1 & u_0 = u_x^\infty & N_{xy} = 0 & \\ n_y = 0 & w_{0,x} = 0 & M_{xy} = 0 & \text{on } \Gamma_4 \\ & & Q_x = 0 & \end{array} \tag{26}$$

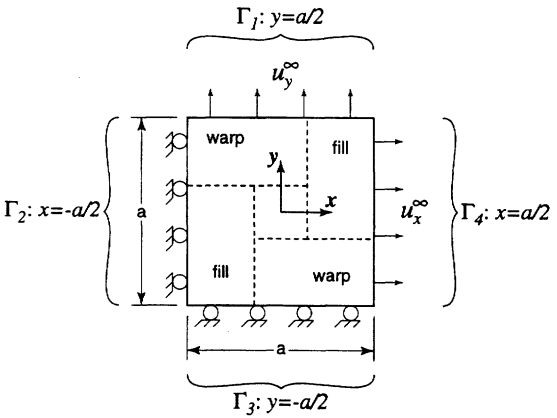

Figure 6. *The plain weave unit-cell subjected to biaxial displacement conditions.*

The uniaxial displacement boundary value problem is defined by exactly the same boundary conditions as the biaxial problem, with the exception that u_y^{∞} is undetermined. As such, the additional equation of global equilibrium is required, which will be discussed in further detail during the solution phase in Section 3.2.

The simple shear boundary value problem is modeled with antisymmetry conditions applied along three edges of the unit-cell shown in Figure 7, and a uniform displacement in the x direction enforced along the top edge. The complete set of boundary conditions are

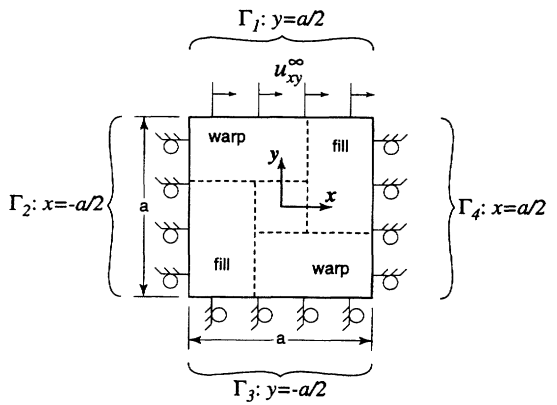

Figure 7. *The plain-weave unit-cell subjected to in-plane shear conditions.*

$$\begin{matrix} n_x = 0 \\ n_y = +1 \end{matrix} \quad u_0 = u_{xy}^{\infty} \quad \begin{matrix} N_y = 0 \\ M_y = 0 \\ M_{xy} = 0 \\ Q_y = 0 \end{matrix} \quad \text{on } \Gamma_1 \tag{27}$$

$$\begin{matrix} n_x = -1 \\ n_y = 0 \end{matrix} \quad v_0 = 0 \quad \begin{matrix} N_x = 0 \\ M_x = 0 \\ M_{xy} = 0 \\ Q_x = 0 \end{matrix} \quad \text{on } \Gamma_2 \tag{28}$$

$$\begin{matrix} n_x = 0 \\ n_y = -1 \end{matrix} \quad u_0 = 0 \quad \begin{matrix} N_y = 0 \\ M_y = 0 \\ M_{xy} = 0 \\ Q_y = 0 \end{matrix} \quad \text{on } \Gamma_3 \tag{29}$$

$$\begin{matrix} n_x = +1 \\ n_y = 0 \end{matrix} \quad v_0 = 0 \quad \begin{matrix} N_x = 0 \\ M_x = 0 \\ M_{xy} = 0 \\ Q_x = 0 \end{matrix} \quad \text{on } \Gamma_4 \tag{30}$$

The boundary conditions for each problem may be used to reduce the variational statement given in Equation (20). For each essential condition that is specified, whether zero or nonzero, the respective variational term is zero in the same domain. For both the biaxial and simple shear sets of boundary conditions, the boundary integral term of Equation (20) becomes zero

$$-\oint_{\Gamma} \{(N_x n_x + N_{xy} n_y)\delta u_0 + (N_{xy} n_x + N_y n_y)\delta v_0 + (Q_x n_x + Q_y n_y)\delta w_0$$

$$- (M_x n_x + M_{xy} n_x)\delta w_{0,x} - (M_{xy} n_x + M_y n_y)\delta w_{0,y}\} dp = 0 \tag{31}$$

and the statement of the principle of virtual work for the problem considered herein is reduced to

$$\delta\Pi = \int_{\Omega} \{N_x \delta u_{0,x} + N_{xy}(\delta u_{0,y} + \delta v_{0,x}) + N_y \delta v_{0,y}$$

$$- M_x \delta w_{0,xx} - 2M_{xy}\delta w_{0,xy} - M_y \delta w_{0,yy} + k_m w_0 \delta w_0\} d\mathcal{A} = 0 \tag{32}$$

The above equation, in conjunction with the appropriate boundary conditions and Equations (3) and (6) may be solved to determine the variation in the micro-field quantities given in Equation (14) through out the domain of the unit-cell. In the next section we employ the Rayleigh-Ritz method of approximation to obtain solutions for the three boundary value problems considered herein.

3. RAYLEIGH-RITZ METHOD OF APPROXIMATION

In the Rayleigh-Ritz method the displacement solutions are approximated by finite linear combinations of the form

$$u_0 = \sum_{j=1}^{n} a_j \psi_u^j + \psi_u^0$$

$$v_0 = \sum_{j=1}^{n} b_j \psi_v^j + \psi_v^0 \tag{33}$$

$$w_0 = \sum_{j=1}^{n} c_j \psi_w^j + \psi_w^0$$

and the unknown constant coefficients a_j, b_j, and c_j are determined by requiring that the principle of virtual work holds for arbitrary variations in the virtual displacements. In Equations (33), $\psi_u^j, \psi_v^j, \psi_w^j$ are functions of x and y and are chosen to satisfy three conditions. The functions must (1) be sufficiently differentiable, (2) satisfy at least the homogeneous form of the specified boundary conditions on u_0, v_0, and w_0, and (3) be linearly independent and complete. The terms ψ_u^0, ψ_v^0, and ψ_w^0 are chosen to satisfy the specified boundary conditions imposed on u_0, v_0, and w_0. The approximate series solutions are substituted into the variational statement of the problem given by

$$\delta\Pi(u_0, v_0, w_0) = 0 \tag{34}$$

which, after expansion in terms of the unknown coefficients, yields

$$\delta\Pi(a_1, a_2, \ldots, a_n, b_1, b_2, \ldots, b_n, c_1, c_2, \ldots, c_n) =$$

$$\sum_{i=1}^{n} \left(\frac{\partial \Pi}{\partial a_i} \delta a_i + \frac{\partial \Pi}{\partial b_i} \delta b_i + \frac{\partial \Pi}{\partial c_i} \delta c_i \right) = 0 \tag{35}$$

where δa_i, δb_i, and δc_i, are arbitrary and independent variations imposed on the constants a_i, b_i, and c_i respectively. As a result,

$$\frac{\partial \Pi}{\partial a_i} = 0 \quad \frac{\partial \Pi}{\partial b_i} = 0 \quad \frac{\partial \Pi}{\partial c_i} = 0 \tag{36}$$

which are $3n$ linearly independent equations in $3n$ unknowns (the Ritz coefficients).

For the solution of the two-dimensional problems considered herein, the series solutions are cast in the following double series form:

$$u_0 = \sum_{m=1}^{M}\sum_{n=1}^{N} a_{mn}\psi_u^{mn} + \psi_u^0$$

$$v_0 = \sum_{m=1}^{M}\sum_{n=1}^{N} b_{mn}\psi_v^{mn} + \psi_v^0 \tag{37}$$

$$w_0 = \sum_{m=1}^{M}\sum_{n=1}^{N} c_{mn}\psi_w^{mn} + \psi_w^0$$

where the Ritz parameters M and N limit the number of terms in the series solutions to $M \times N + 1$. In this paper, M and N are always selected to be equal in order to provide equal accuracy of the solutions in both the x and y directions. Also in Equation (37), a_{mn}, b_{mn}, and c_{mn} represent unknown constants to be determined as part of the energy minimization principle. The variations in the displacements are written with the aid of the chain rule as follows:

$$\delta u_0 = \sum_{i=1}^{M}\sum_{j=1}^{N} \frac{\partial u_0}{\partial a_{ij}}\delta a_{ij} = \sum_{i=1}^{M}\sum_{j=1}^{N} \psi_u^{ij}\delta a_{ij}$$

$$\delta v_0 = \sum_{i=1}^{M}\sum_{j=1}^{N} \frac{\partial v_0}{\partial b_{ij}}\delta b_{ij} = \sum_{i=1}^{M}\sum_{j=1}^{N} \psi_v^{ij}\delta b_{ij} \tag{38}$$

$$\delta w_0 = \sum_{i=1}^{M}\sum_{j=1}^{N} \frac{\partial w_0}{\partial c_{ij}}\delta c_{ij} = \sum_{i=1}^{M}\sum_{j=1}^{N} \psi_u^{ij}\delta c_{ij}$$

In light of the above displacement variations, Equation (32) takes the form:

$$\sum_{i=1}^{M}\sum_{j=1}^{N}\int_{\Omega}\{(N_x\psi^{ij}_{u,x}+N_{xy}\psi^{ij}_{u,y})\delta a_{ij}+(N_y\psi^{ij}_{v,y}+N_{xy}\psi^{ij}_{v,x})\delta b_{ij}$$

$$-(M_x\psi^{ij}_{w,xx}+2M_{xy}\psi^{ij}_{w,xy}+M_y\psi^{ij}_{w,yy}-k_m w_0\psi^{ij}_{w})\delta c_{ij}\}\,d\mathcal{A}=0 \qquad (39)$$

when enforcing Equations (35) and (36) the above variational form yields the following three independent equations:

$$N_x\psi^{ij}_{u,x}+N_{xy}\psi^{ij}_{u,y}=0$$

$$N_y\psi^{ij}_{v,y}+N_{xy}\psi^{ij}_{v,x}=0 \qquad (40)$$

$$-(M_x\psi^{ij}_{w,xx}+2M_{xy}\psi^{ij}_{w,xy}+M_y\psi^{ij}_{w,yy}-k_m w_0\psi^{ij}_{w})=0$$

Due to the generality of the method employed in their derivation, the above equations apply to planar problems involving tension, shear or a combination of both loadings. The next step in the solution process is the appropriate substitution of Equations (3), (6), and (37) into Equations (40), which would require the use of boundary conditions specific to the loading case considered. As such, the rest of the solutions for each problem differ and will be addressed separately. First we shall consider the woven composite plate problem subjected to remote biaxial displacement boundary conditions.

3.1 Biaxial Displacement Boundary Value Problem

The boundary conditions of the biaxial displacement problem shown in Figure 6 are outlined in Section 2.4. In order to conform with the restrictions imposed on the approximate solutions by the Ritz method, the specified functions ψ^0_u, ψ^0_v, and ψ^0_w are chosen as follows:

$$\psi^0_u=u^{\infty}_x\left(\frac{x}{a}+\frac{1}{2}\right)$$

$$\psi^0_v=u^{\infty}_y\left(\frac{y}{a}+\frac{1}{2}\right) \qquad (41)$$

$$\psi^0_w=0$$

In light of the above, Equations (37) take the form

$$u_0 = \sum_{m=1}^{M}\sum_{n=1}^{N} a_{mn}\psi_u^{mn} + u_x^{\infty}\left(\frac{x}{a}+\frac{1}{2}\right)$$

$$v_0 = \sum_{m=1}^{M}\sum_{n=1}^{N} b_{mn}\psi_v^{mn} + u_y^{\infty}\left(\frac{y}{a}+\frac{1}{2}\right) \tag{42}$$

$$w_0 = \sum_{m=1}^{M}\sum_{n=1}^{N} c_{mn}\psi_w^{mn}$$

Appropriate substitution of Equations (3) and (6) casts Equation (40) in terms of u_0, v_0, and w_0, and the above form of the series solution is substituted. The coefficients of the unknown constants a_{mn}, b_{mn}, and c_{mn} are collected to yield the following system of linear equations:

$$\sum_{m=1}^{M}\sum_{n=1}^{N}(K_{11}^{ijmn}a_{mn} + K_{12}^{ijmn}b_{mn} + K_{13}^{ijmn}c_{mn}) = F_1^{ij}$$

$$\sum_{m=1}^{M}\sum_{n=1}^{N}(K_{21}^{ijmn}a_{mn} + K_{22}^{ijmn}b_{mn} + K_{23}^{ijmn}c_{mn}) = F_2^{ij} \tag{43}$$

$$\sum_{m=1}^{M}\sum_{n=1}^{N}(K_{31}^{ijmn}a_{mn} + K_{32}^{ijmn}b_{mn} + K_{33}^{ijmn}c_{mn}) = F_3^{ij}$$

The above system of equations may be written in the matrix form:

$$\begin{bmatrix} [K_{11}^{ijmn}] & [K_{12}^{ijmn}] & [K_{13}^{ijmn}] \\ [K_{21}^{ijmn}] & [K_{22}^{ijmn}] & [K_{23}^{ijmn}] \\ [K_{31}^{ijmn}] & [K_{32}^{ijmn}] & [K_{33}^{ijmn}] \end{bmatrix} \begin{Bmatrix} \{a_{mn}\} \\ \{b_{mn}\} \\ \{c_{mn}\} \end{Bmatrix} = \begin{Bmatrix} \{F_1^{ij}\} \\ \{F_2^{ij}\} \\ \{F_3^{ij}\} \end{Bmatrix} \tag{44}$$

where the superscripts i and j correspond with those of Equation (40), and the super- and subscripts m and n are introduced from the summation in Equation (42). The double index notation is used to represent a vector, and the quadruple index notation represents a two-dimensional matrix. For example, the vectors $\{a_{mn}\}$ and $\{F_1^{ij}\}$ for the number of Ritz parameters $M = N = 2$ are expanded as

$$\{a_{mn}\}=\begin{Bmatrix} a_{11} \\ a_{12} \\ a_{21} \\ a_{22} \end{Bmatrix} \qquad \{F_1^{ij}\}=\begin{Bmatrix} F_1^{11} \\ F_1^{12} \\ F_1^{21} \\ F_1^{22} \end{Bmatrix} \tag{45}$$

and the matrix $[K_{11}^{ijmn}]$ for $M = N = 2$ is

$$[K_{11}^{ijmn}]=\begin{bmatrix} K_{11}^{1111} & K_{11}^{1112} & K_{11}^{1121} & K_{11}^{1122} \\ K_{11}^{1211} & K_{11}^{1212} & K_{11}^{1221} & K_{11}^{1222} \\ K_{11}^{2111} & K_{11}^{2112} & K_{11}^{2121} & K_{11}^{2122} \\ K_{11}^{2211} & K_{11}^{2212} & K_{11}^{2221} & K_{11}^{2222} \end{bmatrix} \tag{46}$$

The global stiffness matrix $[K]$ on the left hand side of Equation (44) is symmetric. As a result the sub-matrices along the diagonal are also symmetric such that:

$$[K_{11}^{ijmn}]=[K_{11}^{ijmn}]^T \qquad [K_{22}^{ijmn}]=[K_{22}^{ijmn}]^T \qquad [K_{33}^{ijmn}]=[K_{33}^{ijmn}]^T \tag{47}$$

At the same time, the off diagonal sub-matrices are not symmetric, but obey the following relationships:

$$[K_{12}^{ijmn}]=[K_{21}^{ijmn}]^T \qquad [K_{13}^{ijmn}]=[K_{31}^{ijmn}]^T \qquad [K_{23}^{ijmn}]=[K_{32}^{ijmn}]^T \tag{48}$$

The global K terms of Equations (43) and (44) are given by:

$$\begin{aligned}
K_{11}^{ijmn} &= \int_\Omega \{\psi_{u,x}^{ij}\psi_{u,x}^{mn} A_{11} + \psi_{u,y}^{ij}\psi_{u,y}^{mn} A_{66}\} d\mathcal{A} \\
K_{12}^{ijmn} &= \int_\Omega \{\psi_{u,x}^{ij}\psi_{v,y}^{mn} A_{12} + \psi_{u,y}^{ij}\psi_{v,x}^{mn} A_{66}\} d\mathcal{A} \\
K_{13}^{ijmn} &= -\int_\Omega \{\psi_{u,x}^{ij}(\psi_{w,xx}^{mn} B_{11} + \psi_{w,yy}^{mn} B_{12}) + 2\psi_{u,y}^{ij}\psi_{w,xy}^{mn} B_{66}\} d\mathcal{A} \\
K_{22}^{ijmn} &= \int_\Omega \{\psi_{v,y}^{ij}\psi_{v,y}^{mn} A_{22} + \psi_{v,x}^{ij}\psi_{v,x}^{mn} A_{66}\} d\mathcal{A} \\
K_{23}^{ijmn} &= -\int_\Omega \{\psi_{v,y}^{ij}(\psi_{w,xx}^{mn} B_{12} + \psi_{w,yy}^{mn} B_{22}) + 2\psi_{v,x}^{ij}\psi_{w,xy}^{\mu\nu} B_{66}\} d\mathcal{A} \\
K_{33}^{ijmn} &= \int_\Omega \{\psi_{w,xx}^{ij}(\psi_{w,xx}^{mn} D_{11} + \psi_{w,yy}^{mn} D_{12}) + 4\psi_{w,xy}^{ij}\psi_{w,xy}^{mn} D_{66} \\
&\quad + \psi_{w,yy}^{ij}(\psi_{w,xx}^{mn} D_{21} + \psi_{w,yy}^{mn} D_{22}) + \psi_{w}^{ij}\psi_{w}^{mn} k_m\} d\mathcal{A}
\end{aligned} \tag{49}$$

whereas the global F terms take the form:

$$F_1^{ij} = -\int_\Omega \{\psi_{u,x}^{ij}(A_{11}u_x^\infty + A_{12}u_y^\infty)\}d\mathcal{A}$$

$$F_2^{ij} = -\int_\Omega \{\psi_{v,y}^{ij}(A_{12}u_x^\infty + A_{22}u_y^\infty)\}d\mathcal{A} \tag{50}$$

$$F_3^{ij} = \int_\Omega \{\psi_{w,xx}^{ij}(B_{11}u_x^\infty + B_{12}u_y^\infty) + \psi_{w,yy}^{ij}(B_{12}u_x^\infty + B_{22}u_x^\infty)\}d\mathcal{A}$$

To obtain a solution for the unknown constants, appropriate shape functions ψ_u^{mn}, ψ_v^{mn} and ψ_w^{mn} must be constructed. In the biaxial displacement problem, an additional constraint may be employed to improve the solution convergence. From Equation (6) we have the following relationships:

$$\begin{aligned} N_{xy} &= A_{66}\gamma_{xy}^0 + B_{66}\kappa_{xy}^0 \\ M_{xy} &= B_{66}\gamma_{xy}^0 + D_{66}\kappa_{xy}^0 \end{aligned} \tag{51}$$

where, for the biaxial problem, N_{xy} and M_{xy} equal zero everywhere on Γ. Solving the above system of equations for γ_{xy}^0 and κ_{xy}^0 results in

$$\gamma_{xy}^0 = \kappa_{xy}^0 = 0 \quad \text{on} \quad \Gamma \tag{52}$$

As such, a set of linear independent functions which satisfy the homogeneous boundary conditions and the above constraint is

$$\begin{aligned} \psi_u^{mn} &= \sin\left[2m\pi\frac{x}{a}\right]\cos\left[2(n-1)\pi\frac{y}{a}\right] \\ \psi_v^{mn} &= \cos\left[2(m-1)\pi\frac{x}{a}\right]\sin\left[2n\pi\frac{y}{a}\right] \\ \psi_w^{mn} &= \sin\left[(2m-1)\pi\frac{x}{a}\right]\sin\left[(2n-1)\pi\frac{y}{a}\right] \end{aligned} \tag{53}$$

The above set of shape functions include only certain even and odd terms. The coefficients of the excluded terms will be zero due to the particular construction of the plain weave architecture, and are hence omitted to improve convergence.

After substitution of Equation (53), the global K and global F terms of Equations (49) and (50) may be integrated numerically, and the linear system of

Equations (44) may be solved for the Ritz coefficients a_{mn}, b_{mn}, and c_{mn}. Equation (42) in conjunction with Equation (53) then yields continuous expressions for the mid-plane displacement results, and can be used to compute the mid-plane strains and curvatures with Equation (3). The two-dimensional strains at a point may be determined from Equation (2), and the corresponding stresses at a point in a layer are found using Equation (1). Hence, the complete solution of the two-dimensional plain weave biaxial displacement boundary value problem is known.

3.2 Uniaxial Displacement Boundary Value Problem

Another important loading configuration of the woven unit-cell is the uniaxial displacement problem. Both the effective Young's modulus and Poisson's ratio (discussed at the end of this section) of the woven unit-cell may be determined from the solution of this problem. The boundary conditions of the uniaxial problem are identical to those of the biaxial displacement problem and are given by Equations (23–26). As a result, the finite series solution takes the same form as Equations (42) and (53). However, for uniaxial loading, the uniform displacement in the y direction u_y^∞ is unknown and an additional equation is required for the solution. In order to solve for u_y^∞ we employ the global equilibrium equation along the top edge given by

$$\int_{-a/2}^{a/2} N_y(x, y)|_{y=a/2}\, dx = 0 \tag{54}$$

The resulting system of equations with u_y^∞ treated as an unknown is:

$$\begin{aligned}
\sum_{m=1}^{M}\sum_{n=1}^{N}(K_{11}^{ijmn}a_{mn} + K_{12}^{ijmn}b_{mn} + K_{13}^{ijmn}c_{mn} + K_{14}^{ij}u_y^\infty) &= F_1^{ij} \\
\sum_{m=1}^{M}\sum_{n=1}^{N}(K_{21}^{ijmn}a_{mn} + K_{22}^{ijmn}b_{mn} + K_{23}^{ijmn}c_{mn} + K_{24}^{ij}u_y^\infty) &= F_2^{ij} \\
\sum_{m=1}^{M}\sum_{n=1}^{N}(K_{31}^{ijmn}a_{mn} + K_{32}^{ijmn}b_{mn} + K_{33}^{ijmn}c_{mn} + K_{34}^{ij}u_y^\infty) &= F_3^{ij} \\
\sum_{m=1}^{M}\sum_{n=1}^{N}(K_{41}^{mn}a_{mn} + K_{42}^{mn}b_{mn} + K_{43}^{mn}c_{mn} + K_{44}u_y^\infty) &= F_4
\end{aligned} \tag{55}$$

where the last equation results from the global equilibrium Equation (54). The above equations may be written in the matrix form as follows:

$$\begin{bmatrix} [K_{11}^{ijmn}] & [K_{12}^{ijmn}] & [K_{13}^{ijmn}] & \{K_{14}^{ij}\} \\ [K_{21}^{ijmn}] & [K_{22}^{ijmn}] & [K_{23}^{ijmn}] & \{K_{24}^{ij}\} \\ [K_{31}^{ijmn}] & [K_{32}^{ijmn}] & [K_{33}^{ijmn}] & \{K_{34}^{ij}\} \\ \{K_{41}^{mn}\}^T & \{K_{42}^{mn}\}^T & \{K_{43}^{mn}\}^T & K_{44} \end{bmatrix} \begin{Bmatrix} \{a_{mn}\} \\ \{b_{mn}\} \\ \{c_{mn}\} \\ u_y^{\infty} \end{Bmatrix} = \begin{Bmatrix} \{F_1^{ij}\} \\ \{F_2^{ij}\} \\ \{F_3^{ij}\} \\ \{F_4\} \end{Bmatrix} \tag{56}$$

The global K terms given by Equation (49) for the biaxial displacement problem are the same for this problem and the additional global K terms in Equation (56) are

$$\begin{aligned} K_{14}^{ij} &= \int_{\Omega} \psi_{u,x}^{ij} A_{12}\, dA & K_{41}^{mn} &= \int_{\Gamma_1} \psi_{u,x}^{mn} A_{12}\, dp \\ K_{24}^{ij} &= \int_{\Omega} \psi_{v,y}^{ij} A_{22}\, dA & K_{42}^{mn} &= \int_{\Gamma_1} \psi_{v,y}^{mn} A_{22}\, dp \\ K_{34}^{ij} &= \int_{\Omega} \psi_{w,xx}^{ij} B_{12} + \psi_{w,yy}^{ij} B_{22}\, dA & K_{43}^{mn} &= \int_{\Gamma_1} (\psi_{w,xx}^{mn} B_{12} + \psi_{w,yy}^{mn} B_{22})\, dp \end{aligned} \tag{57}$$

$$K_{44}^{mn} = \int_{\Gamma_1} A_{22}\, dp$$

where the integral over the boundary Γ_1 for an arbitrary integrated $f(x,y)$ represents the integral

$$\int_{\Gamma_1} f(x,y)dp \rightarrow \int_{-a/2}^{a/2} f(x,y)|_{y=a/2}\, dx \tag{58}$$

The global F terms of Equation (56) also differ from those of the biaxial problem and are given as follows:

$$\begin{aligned} F_1^{ij} &= -\int_{\Omega} \psi_{u,x}^{ij} A_{11}\, u_x^{\infty}\, dA \\ F_2^{ij} &= -\int_{\Omega} \psi_{v,y}^{ij} A_{12}\, u_x^{\infty}\, dA \\ F_3^{ij} &= \int_{\Omega} \{\psi_{w,xx}^{ij} B_{11} + \psi_{w,yy}^{ij} B_{12}\} u_x^{\infty}\, dA \\ F_4 &= -\int_{\Gamma_1} A_{12}\, u_x^{\infty}\, dp \end{aligned} \tag{59}$$

Solution of the $3 \times M \times N \times 1$ equations of Equation (56) yields the values for the $3 \times M \times N$ Ritz coefficients plus the uniform displacement u_y^∞ of the top edge of the unit-cell. These quantities along with the applied displacement u_x^∞ may be substituted into Equation (42) and in conjunction with Equation (53) result in the solution for the mid-plane displacements throughout the domain of the unit-cell. These field equations together with the elasticity relationships given in Section 2.1 may be used to fully characterize the two-dimensional micro-stress and micro-strain behavior of the woven unit-cell.

The solution to the uniaxial boundary value problem outlined in this section may be used to determine two of the in-plane effective orthotropic linear elastic properties of the woven unit-cell. The effective Young's modulus E_x in the loading direction is

$$E_x = \frac{F_x}{A_4 \varepsilon_x} = \frac{F_x}{h u_x^\infty} \tag{60}$$

where $A_4 = ah$ is the area of the face corresponding with the boundary Γ_4, $\varepsilon_x = u_x^\infty / a$ is the strain in the loading direction, and the total force F_x in the loading direction is computed from

$$F_x = \int_{-a/2}^{a/2} N_x(a/2, y) dy \tag{61}$$

The effective Poisson's ratio ν_{xy} is computed with the aid of the displacement in the y direction u_y^∞ and is

$$\nu_{xy} = -\frac{\varepsilon_y}{\varepsilon_x} = -\frac{u_y^\infty}{u_x^\infty} \tag{62}$$

The plain weave unit-cell is in general orthotropic, and as such, additional material constants are required to characterize the overall constitutive response to applied loading. The Young's modulus in the y direction E_y for hybrid composites may be computed by specifying u_y^∞ and solving for u_x^∞ in the manner presented above. In this paper we limit the discussion to non-hybrid woven composites, in which case $E_y = E_x$. Even non-hybrid composites may exhibit off axis orthotropic behavior and as a result the effective shear modulus G_{xy} must be computed. In the next section we present the approximate solution to the simple shear problem, which may be employed as one component in combined loading analysis and also yields the effective unit-cell shear modulus G_{xy}.

3.3 Simple Shear Boundary Value Problem

The simple shear problem may be solved using an approach similar to that used in the previous two sections. Initially, shape functions which satisfy the specified boundary conditions are selected, and the finite series solution is substituted into the principle of virtual work. Subsequently, an appropriate form of the shape functions which satisfy the homogeneous form of the specified boundary conditions are developed. In the simple shear problem the specified essential boundary conditions shown schematically in Figure 7 and presented mathematically in Equations (27–30) are satisfied by requiring that,

$$\psi_u^0 = u_{xy}^\infty \left(\frac{y}{a} + \frac{1}{2}\right)$$

$$\psi_v^0 = 0 \tag{63}$$

$$\psi_w^0 = 0$$

Consequently, the finite series solution takes the form

$$u_0 = \sum_{m=1}^{M}\sum_{n=1}^{N} a_{mn}\psi_u^{mn} + u_{xy}^\infty \left(\frac{y}{a} + \frac{1}{2}\right)$$

$$v_0 = \sum_{m=1}^{M}\sum_{n=1}^{N} b_{mn}\psi_v^{mn} \tag{64}$$

$$w_0 = \sum_{m=1}^{M}\sum_{n=1}^{N} c_{mn}\psi_w^{mn}$$

Substitution of Equation (64) into the principle of virtual work results in a system of linear equations in the same form as equation (44) with global K terms identical to those given in Equation (49) and global F terms given by

$$F_1^{ij} = -\int_\Omega \psi_{u,y}^{ij} A_{66} u_{xy}^\infty \, d\mathcal{A}$$

$$F_2^{ij} = -\int_\Omega \psi_{v,x}^{ij} A_{66} u_{xy}^\infty \, d\mathcal{A} \tag{65}$$

$$F_3^{ij} = \int_\Omega 2\psi_{w,xy}^{ij} B_{66} u_{xy}^\infty \, d\mathcal{A}$$

Based on the criteria outlined earlier, the shape functions chosen to satisfy the homogeneous essential simple shear boundary conditions are

$$\psi_u^{mn} = \cos\left[2(m-1)\pi\frac{x}{a}\right]\sin\left[2n\pi\frac{y}{a}\right]$$

$$\psi_v^{mn} = \sin\left[2m\pi\frac{x}{a}\right]\cos\left[2(n-1)\pi\frac{y}{a}\right] \tag{66}$$

$$\psi_w^{mn} = \cos\left[(2m-1)\pi\frac{x}{a}\right]\cos\left[(2n-1)\pi\frac{y}{a}\right]$$

In the above equations, the coefficients of certain odd functions will be zero, and as such, the terms are dropped. As in the previous two boundary value problems, the finite series yields an approximate solution for the displacement fields, and the corresponding micro-stresses and micro-strains may be computed with the aid of the relationships presented in Section 2.1.

The effective shear modulus G_{xy} of the woven unit-cell may be computed from the approximate solution to the simple shear boundary value problem presented in this section and is given by:

$$G_{xy} = \frac{F_{yx}}{A_1\gamma_{xy}} = \frac{F_{yx}}{hu_{xy}^{\infty}} \tag{67}$$

where $V_1 = ah$ is the area of the unit-cell face corresponding with the boundary Γ_1, and $\gamma_{xy} = u_{xy}^{\infty}/a$ is the overall applied shear strain. The reaction force F_{yx} is computed from the series solution in conjunction with Equation (6) resulting in the integral

$$F_{yx} = \int_{-a/2}^{a/2} N_{xy}(x, a/2)\,dx \tag{68}$$

This concludes the formulation of the approximate finite series solutions to the biaxial displacement, uniaxial displacement, and simple shear plain weave unit-cell boundary value problems. In the next section these formulations will be used to solve the three boundary value problems applied to a *soft*-polymer matrix composite with the porous matrix geometry, and for a *stiff*-ceramic matrix composite with the matrix layer geometry. The solutions will in turn be used to study the convergence of the finite series solutions for increasing number of terms.

4. RAYLEIGH-RITZ SOLUTION CONVERGENCE

The objective of this work is to develop improved generality and accuracy over that of the method of cells [11], and reduce the volume of problem data and computational cost in comparison to the finite element method. As such, it is important to determine an optimal number of terms required in the finite series solutions to yield adequate approximations to the actual solutions. In general, the Rayleigh-Ritz solutions are approximate for a finite number of terms. As the number of terms increases, the accuracy of the solution increases. However, at some point an increase in the number of terms may not result in an appreciable change in the solution. At that point, the solution is said to converge. In the ideal case one would always use enough terms for the solution to converge, because the convergent solution is the most accurate possible for a given series. However, an increase in the number of terms may result in substantial increase in the required computation thus limiting the effectiveness of the solution. In this section we perform solution convergence studies as required for the determination of the significant number of terms in the adopted series solutions.

Recall that in Equations (42) and (64), the number of terms in the finite series solution are specified with the Ritz parameters M and N, in which case there are $M \times N$ terms in the series plus the particular terms satisfying the specified boundary conditions. For the results presented in this section, we select $M = N = k$ and denote this as the kth solution. To investigate the convergence of the solutions for increasing k we compute the percent difference between solution k and $k + 1$ as

$$\text{Solution Improvement Between Terms} = \frac{||\{\varepsilon\}_{k+1} - \{\varepsilon\}_k||}{||\{\varepsilon\}_{k+1}||} \times 100\% \quad (69)$$

where $\{\varepsilon\}$ represents the vector containing the strains given by Equation (2). The norm for an arbitrary vector $\{e\}$ with three components is denoted $||\{e\}||$ and is defined by

$$||\{e\}|| = \left[\int_V \sum_{j=1}^{3} e_j e_j \, dV\right]^{1/2} \quad (70)$$

where V represents the domain of the volume occupied by the woven unit-cell. As indicated above, in Equation (69) the percent difference between solution k and $k + 1$ is computed by taking the appropriate norm of the mid-plane strains and curvatures such that $\{e\} \equiv \{\varepsilon\}$. The respective strain vector $\{\varepsilon\}$ for solution k denoted $\{\varepsilon\}_k$ is

$$\{\varepsilon\}_k = \begin{Bmatrix} \varepsilon_x \\ \varepsilon_y \\ \gamma_{xy} \end{Bmatrix}_k \tag{71}$$

The spatially varying local strain components ε_x, ε_y, and γ_{xy} are computed from the mid-plane strains and curvatures via Equation (2). Here the strains are used to plot the convergence because these quantities are used in the prediction of micro-stresses and are thus important for the prediction of micro-damage. It is also recognized that, the strains being secondary variables, are expected to converge more slowly than the displacements.

In addition to the above solution convergence studies, and in order to obtain a measure of the overall accuracy of the solution, we shall also calculate for every solution k an estimated error norm as follows:

$$\text{Estimated Solution Error} = \frac{||\{\varepsilon\}_{ref} - \{\varepsilon\}_k||}{||\{\varepsilon\}_{ref}||} \times 100\% \tag{72}$$

where $\{\varepsilon\}_{ref}$ represents the reference strains obtained from a solution comprised of $M = N = k = 20$ series terms and integrated using a robust 150 × 150 Gauss integration grid over the domain of the unit-cell for *soft*-polymer matrix systems, or a 40 × 40 Gauss integration grid within each of the eight sub-elements for *stiff*-ceramic matrix systems. As will be discussed later on in this work, the error norms given by Equations (69) and (72) will be plotted against the number of series terms k for both *soft*-polymer and *stiff*-matrix woven composites under uniaxial, biaxial and pure shear in-plane loading. It is important to note however, that the error norm given by Equation (72), does not account for the presence of out-of-plane strains. In addition, since the reference state of strain in Equation (72) is obtained using the same method, the above error reflects mostly an estimate of how good the kth solution is relative to the reference solution which is obtained by exploring most of the method's capabilities. However, full 3-D error estimates obtained by comparing the predictions of the method developed herein with 3-D finite element results are presented in References [44,45] and are beyond the scope of this work.

The variables associated with the equations presented in the formulation of the boundary value problems are non-dimensionalized in accordance with the scheme presented in the Appendix. In all cases the characteristic length L_c and modulus E_c are chosen as the tow undulation half period a and the tow longitudinal modulus E_1, respectively, such that $\hat{a} = 1.0$ and $\hat{E}_1 = 1.0$. For the biaxial and uniaxial displacement problems the characteristic displacement u_c is set equal to the applied displacement in the x direction u_x^∞, resulting in $\hat{u}_x^\infty = 1.0$. In the case of in-plane shear loading, $u_c = u_{xy}^\infty$ resulting in $\hat{u}_{xy}^\infty = 1.0$.

In the following sections we will explore the convergence of the Rayleigh-Ritz solutions of the three boundary value problems outlined earlier for two different systems. One system consists of geometry and material properties characteristic of *soft*-polymer matrix woven composites, and the other is comprised of the geometry and a set of material properties characteristic of *stiff*-ceramic matrix woven composites. First we shall consider the *soft*-polymer matrix system. In this work, only the results required to establish the convergence and accuracy of the solutions are presented. More extensive results which include micro-stress field comparisons between the current method and 3-D finite elements as well as parametric effective property studies are presented in References [46,47].

4.1 *Soft*-Polymer Matrix Composite Results

The geometry of typical plain weave fabric *soft*-polymer matrix composites corresponds with that of the porous matrix model shown in Figure 1(a), with geometry parameters a, b, g, h, and l as shown in Figure 3. For the symmetric unit-cell shown in Figure 1(a) the length l is set equal to the undulation half period a, and the geometry parameters are non-dimensionalized via Equations (A6). The matrix layer thickness t does not apply to the porous matrix model because the inter-tow regions are filled completely with matrix material. This material may, however, contain dispersed microporosity which effectively reduces the overall elastic properties of the matrix material with material properties $E_{\bar{m}}$ and $\nu_{\bar{m}}$. The transversely isotropic tows, with effective properties E_1, E_2, ν_{12},ν_{23}, and G_{12}, may be comprised of microconstituents such as fibers and matrix material. The effective tow and matrix moduli are non-dimensionalized via Equations (A8) and (A9), respectively. The non-dimensional numerical values used to represent a *soft*-polymer matrix woven composite geometry and material properties are listed in Table 1. The parameters presented in the table represent nominal values typical of *soft*-polymer matrix woven composite configurations and on the same order as those employed by Naik and Shembekar in Reference [6]. The volume fractions of inter-tow matrix and fill and warp tows were computed by numerical

Table 1. Non-dimensional input parameters and overall volume fractions of the tows and matrix characteristic of a soft-polymer matrix plain weave fabric composite.

Geometry	Effective Tow	Effective Matrix	Overall Volume Fractions
$\hat{a} = 1.0$	$\hat{E}_{11} = 1.0$		
$\hat{b} = 0.1$	$\hat{E}_{22} = 0.08$		$V_{fill} = 0.319$
$\hat{g} = 0.0$	$\nu_{12} = 0.28$	$\hat{E}_{\bar{m}} = 0.02$	$V_{warp} = 0.319$
$\hat{h} = 0.2$	$\nu_{23} = 0.38$	$\nu_{\bar{m}} = 0.35$	$V_{matrix} = 0.362$
$\hat{l} = 1.0$	$\hat{G}_{12} = 0.04$		

integration of the volume of each phase with the aid of the geometry surface functions given in section 2.2. In the ensuing analysis, the effective elastic foundation stiffness k_m is assigned a value of zero, and hence, only a single woven ply is considered.

A computer FORTRAN program called "WOVENCELL.F" was developed to solve the three boundary value problems for both the porous matrix and matrix layer geometry models with the effective tow and matrix material properties as input. In the program, one-dimensional integrals associated with the global K and F terms are evaluated using a Gauss integration scheme. Automated modules allowing the use of user defined number of integration points have been incorporated. Similarly, the associated two-dimensional integrals are also evaluated using a two-dimensional Gauss integration scheme wherein the user is allowed to input the number of integration grid points in the x and y orthogonal directions of the woven unit cell. The above integration scheme was employed in seeking solutions for *soft*-polymer matrix woven systems. Results for a 40 × 40, 50 × 50 and 100 × 100 unit-cell integration grid are reported in this paper for *soft*-polymer woven composites. However, as will be seen later on in this work, a slightly different integration scheme was employed in the case of *stiff*-ceramic matrix systems as needed to better account for the expected stress concentrations in the near vicinity of the hole at the center of the unit cell.

The resulting systems of linear equations given by Equations (44) and (56) are solved for the Ritz coefficients $\hat{a}_{mn}$, $\hat{b}_{mn}$, and $\hat{c}_{mn}$, in the case of uniaxial displacement, the unknown y displacement $\hat{u}_y^{\infty}$ using direct Gaussian elimination. The computer program was used to solve the three boundary value problems for the input parameters given in Table 1 for the Ritz parameters $M = N = 3$, and the resulting non-dimensional Ritz coefficients are tabulated in Table 2. In the case of uniaxial displacement, the non-dimensional unknown displacement in the y direction $\hat{u}_y^{\infty}$ is listed at the top of Table 2(a).

In each load case, the Ritz coefficients $\hat{a}_{mn}$ are of similar magnitudes but they assume different values for different mn combination pairs. While the same is true for $\hat{b}_{mn}$, there is an interesting trend in the $\hat{c}_{mn}$ coefficients. For the cases of biaxial displacement and simple shear the coefficients $\hat{c}_{11}$, $\hat{c}_{22}$, and $\hat{c}_{33}$ are all approximately equal to zero. Additionally, the remaining terms appear to obey the relationship $\hat{c}_{mn} = -\hat{c}_{nm}$. In light of these trends, the shape functions were rewritten, eliminating the terms with zero coefficients and combining terms with like coefficients. The new shape functions were used to solve the boundary value problems and the solutions were compared. The new shape functions did not appear to improve the solutions, nor did they appear to improve the convergence. They were also significantly more complex, and as a result, were not utilized in the analysis.

The results for the solution improvement between terms represented by Equation (69) as well as the error norm given by Equation (72) for the kth solution are presented on the left and right columns in Figure 8 for the input listed in Table 1. Results for uniaxial, biaxial and pure shear loading are presented. For each case, the kth solution, i.e., the solution comprised of $M = N = k$ number of series terms,

Table 2. Non-dimensional coefficients of the Rayleigh-Ritz finite series solutions for the three loading cases, applied to the soft-polymer matrix plain weave fabric composite with geometry and properties given in Table 1.

PMC Ritz Coefficients ($M = N = 3$)			
(a) Uniaxial Displacement $\hat{u}_y^{\infty} = -0.2396$			
mn	$\hat{a}_{mn}$	$\hat{b}_{mn}$	$\hat{c}_{mn}$
11	0.1385E−01	0.1568E−01	0.1171E+01
12	0.1822E−01	0.2813E−02	0.3798E−01
13	0.3259E−02	0.4393E−03	0.2347E−02
21	−0.1143E−02	−0.1602E−01	0.3649E−01
22	0.2971E−02	−0.2060E−02	0.2927E−02
23	0.9945E−03	−0.2393E−03	0.1732E−03
31	−0.1297E−03	−0.2575E−02	0.2825E−02
32	0.5508E−03	−0.6299E−03	0.4566E−03
33	0.2346E−03	−0.4242E−04	0.1092E−03
(b) Biaxial Displacement			
mn	$\hat{a}_{mn}$	$\hat{b}_{mn}$	$\hat{c}_{mn}$
11	0.3870E−01	0.3870E−01	−0.9572E−15
12	0.2884E−02	0.2189E−02	0.1951E−02
13	0.8957E−03	0.4057E−03	−0.6270E−03
21	0.2189E−02	0.2884E−02	0.1951E−02
22	0.1194E−02	0.1194E−02	−0.4864E−16
23	0.4778E−03	0.4082E−03	−0.3714E−03
31	0.4057E−03	0.8957E−03	0.6270E−03
32	0.4082E−03	0.4778E−03	0.3714E−03
33	0.2518E−03	0.2518E−03	0.2273E−16
(c) Simple Shear			
mn	$\hat{a}_{mn}$	$\hat{b}_{mn}$	$\hat{c}_{mn}$
11	0.4291E−01	0.4291E−01	−0.6619E−16
12	0.7400E−02	0.2301E−02	−0.2121E−02
13	0.2260E−02	0.4198E−05	−0.2491E−03
21	0.2301E−02	0.7400E−02	0.2121E−02
22	0.1582E−02	0.1582E−02	−0.3988E−17
23	0.7765E−03	0.1730E−03	−0.9660E−04
31	0.4198E−05	0.2260E−02	0.2491E−03
32	0.1730E−03	0.7765E−03	0.9660E−04
33	0.1282E−03	0.1282E−03	0.7820E−19

was obtained using a 40 × 40, 50 × 50 and 100 × 100 unit-cell integration grid. The uniaxial results are presented in the top row of plots, whereas the biaxial and pure shear results are presented in the second and third row of plots respectively. As shown in Figure 8, both the solution improvement norm as well as the estimated solution error norm decrease with the number of series terms k increases. A dramatic drop in both norms is obtained between solutions comprised of as few as two terms, i.e., $k = 2$ and solutions comprised of six to eight terms. As shown in Figure 8, when a relatively coarse, i.e., 40 × 40, grid of Gauss integration points was used, the uniaxial and biaxial solutions comprised of more than $k = 14$ terms were found to become unstable. The results reported in Figure 8 suggest that when a higher number of series terms is used, a convergent solution can only be obtained by using an improved integration scheme such as the 50 × 50 or 100 × 100 grids of Gauss integration points. This is expected, since the higher series trigonometric terms introduce rapid changes in the solution due to their small wave length. While slightly improving the estimated solution accuracy (see right column in Figure 8),

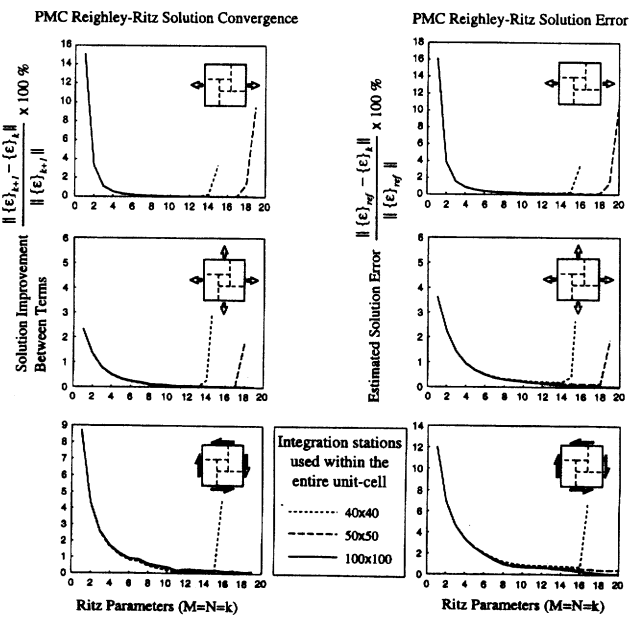

Figure 8. *Left column of plots: Percent difference between consecutive Rayleigh-Ritz solutions as a function of the number of terms used in the series solution. Right column of plots: An estimated error norm of the kth solution relative to a reference solution obtained for M = N = k = 20 using a 150 × 150 grid of Gauss integration points over the unit cell. As shown, results for uniaxial, biaxial and pure shear in-plane loading, are presented. Material and geometry data used for a soft-polymer matrix plain weave fabric composite are those given in Table 1.*

the latter integration schemes lead to substantial increases in the associated computational time. As such, the optimal number of series terms needs to be chosen through a proper evaluation of the trade-offs between accuracy and solution efficiency. The results presented in Figure 8 aim at assisting the user in making that type of decision.

In an effort to achieve a balance between the accuracy of the approximate solutions, their computational cost, and numerical stability, Figure 8 may be used to select an appropriate number of Ritz parameters for future solutions. In all three boundary value problems, a value of $k = 8$ would appear to give satisfactory results. However, a value of $k = 8$ results in the solution of a system of 192 linear equations (193 for uniaxial displacement). While the computation cost in reducing this system of equations is negligible, the solution requires the numerical integration of at least 36,864 integrals associated with the global K and F terms. With 40×40 Gauss point quadrature the computational cost in evaluating these integrals becomes appreciable. A better compromise would be to select $k = 6$, which would yield an acceptable approximation at reduced computational cost.

4.2 *Stiff*-Ceramic Matrix Composite Results

The geometry of the *stiff*-ceramic matrix plain weave fabric composites differ from the system studied in the previous section due to the existence of large scale voids arising from the CVI process. These voids are included in the matrix layer model shown in Figure 1(b). The geometry parameters of the matrix layer model are the same as the porous matrix model with the addition of the matrix layer thickness t as shown in Figure 3. The effective material properties of the transversely isotropic tows are $E_1, E_2, \nu_{12}, \nu_{23}$, and G_{12}, and the material properties of the effective matrix are $E_{\bar{m}}$ and $\nu_{\bar{m}}$. The tows may represent a highly complex microstructure consisting of bundles of fibers, fiber coating, bundle matrix, porosity within the bundles, and coating surrounding the bundles. The homogenization of such microstructure is treated in Reference [23]. All the variables associated with the *stiff*-ceramic matrix system are non-dimensionalized in the same manner as the previous section. The non-dimensional numerical values characteristic of a *stiff*-ceramic matrix composite used in this analysis are presented in Table 3.

Table 3. Non-dimensional input parameters and overall volume fractions of the tows and matrix for a stiff-ceramic matrix plain weave fabric composite.

Geometry	Effective Tow	Effective Matrix	Overall Volume Fractions
$\hat{a} = 1.0$ $\hat{b} = 0.1$ $\hat{g} = 0.15$ $t = 0.03$ $\hat{h} = 0.205$ $\hat{l} = 1.0$	$\hat{E}_1 = 1.0$ $\hat{E}_2 = 0.5$ $\nu_{12} = 0.2$ $\nu_{23} = 0.25$ $\hat{G}_{12} = 0.25$	$\hat{E}_{\bar{m}} = 3.0$ $\nu_{\bar{m}} = 0.3$	$V_{fill} = 0.272$ $V_{warp} = 0.272$ $V_{matrix} = 0.252$ $V_{void} = 0.204$

Due to the presence of the large void in the center of the unit-cell, a domain integration scheme was employed in seeking the solutions for *stiff*-ceramic matrix systems. As shown schematically in Figure 9, the mid-plane of the woven unit-cell is divided into eight sub-domains. Each sub-domain is then mapped onto the isoparametric space using the mapping functions for an eight-noded element. A grid of Gauss integration points is then introduced in the normalized domain consistent with Figure 9 wherein a 10 × 10 grid is shown in association with domain element #1. Micro-stress fields, throughout the unit-cell including the region of stress concentration which were obtained using the method developed herein in conjunction with the above integration scheme were shown to compare very favorably with 3-D finite element predictions (see References [44,47]).

The three boundary value problems were solved using the FORTRAN program discussed in the previous section for the input parameters given in Table 3. The non-dimensional Ritz coefficients for $M = N = 3$ are listed in Table 4. In the case of uniaxial loading, the unknown displacement component $\hat{u}_y^{\infty}$, is included adjacent to the heading of Table 4(a). In this table the Ritz coefficients follow a similar trend to that of the *soft*-polymer matrix composites Ritz coefficients. Several more complex variations of the shape functions that take advantage of the pattern were tested but showed no appreciable computational improvement, as in the previous section.

As in the case of *soft*-polymer systems, the solution improvement and estimated error norms given by Equations (69) and (72) respectively are plotted in Figure 10 as a function of the number of series terms $M = N = k$. As discussed above, in this case the solutions were obtained using the eight domain elements shown in Figure 9. Results for a 10 × 10, 20 × 20, and 40 × 40 grids of Gauss integration points are presented. As in the *soft*-polymer matrix case, the estimated error norm shown on the right column of plots decreases monotonically with increasing k. However, the convergence norm which represents solution improvements between terms, is shown to decrease dramatically as k increases from 2 to 4, then remains either almost constant or slightly increases for k between 4 → 8 and continues to monotonically decrease as k increases at values greater than 8. When using the 10 × 10 per domain element integration scheme, the solutions grow unstable for $k = 6$. When a 20 × 20 per domain element integration scheme is used, the solutions remain stable until $k = 14$. The 40 × 40 integration scheme is shown to assure solution stability for at least $k = 20$ and possibly higher values.

The results presented in Figure 10 suggest that in the case of *stiff*-ceramic matrix woven composites, solution convergence is not as strong as in the *soft*-polymer system case. This slower rate of convergence is to a large extent due to the presence of the large void [see Figure 1(b)] in the center of the matrix layer geometry unit-cell. This hole gives rise to a stress concentration which requires an increased number of terms in the finite series solution. As reported elsewhere Reference [47], the approximate solutions do capture the stress concentrations around the

Table 4. Non-dimensional coefficients of the Rayleigh-Ritz finite series solutions for the three loading cases, applied to the stiff-ceramic matrix plain weave fabric composite with geometry and properties given in Table 3.

CMC Ritz Coefficients ($M = N = 3$)			
(a) Uniaxial Displacement ($\hat{u}_y^{\infty} = -0.2467$)			
mn	$\hat{a}_{mn}$	$\hat{b}_{mn}$	$\hat{c}_{mn}$
11	−0.2394E−02	−0.2915E−02	0.9442E+00
12	0.3442E−01	0.2406E−04	−0.4362E+00
13	−0.9461E−03	0.9683E−04	0.2983E+00
21	0.6942E−02	−0.1430E−01	0.3828E+00
22	−0.1556E−02	0.4193E−04	0.3365E+00
23	0.2648E−02	−0.5148E−04	0.3379E+00
31	0.5540E−03	0.3843E−03	0.6282E+00
32	0.2191E−02	−0.9246E−03	0.1871E+00
33	0.1945E−02	0.1114E−03	0.3044E+00
(b) Biaxial Displacement			
mn	$\hat{a}_{mn}$	$\hat{b}_{mn}$	$\hat{c}_{mn}$
11	−0.7049E+00	−0.7049E−02	−0.3392E−10
12	0.2671E+00	0.9249E−02	−0.5662E−02
13	−0.7458E+00	0.8641E−03	−0.7945E−03
21	0.9249E+00	0.2671E−01	0.5662E−02
22	−0.2010E+00	−0.2010E−02	0.6231E−11
23	0.2288E+00	0.2841E−02	0.2002E−03
31	0.8641E+00	−0.7458E−03	0.7945E−02
32	0.2841E+00	0.2288E−02	−0.2002E−03
33	0.2731E+00	0.2731E−02	06787E−12
(c) Simple Shear			
mn	$\hat{a}_{mn}$	$\hat{b}_{mn}$	$\hat{c}_{mn}$
11	0.2491E+00	0.2491E+00	0.1521E−11
12	0.7212E+00	0.7287E+00	0.3195E−02
13	0.1132E+00	−0.4977E+00	0.1515E−02
21	0.7287E+00	0.7212E+00	−0.3195E−02
22	−0.3905E+00	−0.3905E+00	−0.1395E−11
23	0.1425E+00	0.7670E+00	−0.6540E−05
31	−0.4977E+00	0.1132E+00	−0.1515E−02
32	0.7670E+00	0.1425E+00	0.6540E−05
33	0.1110E+00	0.1110E+00	−0.1313E−12

large cylindrical void in a manner consistent with the 3-D finite element predictions. While these semi-analytical solutions obtained for CVI ceramic matrix composites are somewhat limited as discussed above, they do represent a marked improvement over previous solutions and offer a great deal of insight into the mechanical response of CVI plain-weave ceramic matrix composites (see References [44,47]).

With the above limitations in mind we would like to select an appropriate Ritz parameter $M = N$ which represents a reasonable compromise between accuracy and computational cost for future solutions. For all loading cases considered, the results reported in Figure 10 suggest that highly accurate solutions can be obtained with $M = N = 12$ or 13. However, it is important to note that the associated computations required increase exponentially for increasing M and N. A more appropriate choice would be $M = N = 10$, and a value of $M = N = 8$ would be acceptable. The solution time for $M = N = 8$ is three times that for $M = N = 6$, and as such, in instances where less accuracy is required, $M = N = 6$ may be sufficient.

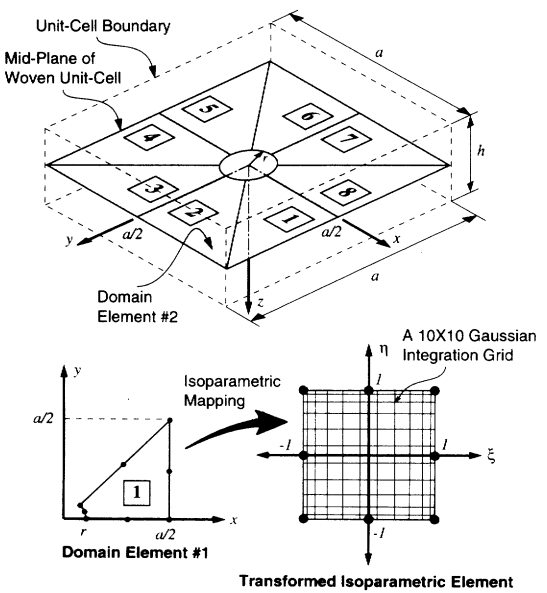

Figure 9. *A schematic of the improved integration scheme employed in the modeling of stiff-ceramic matrix systems. Eight domain elements are mapped to the isoparametric space where a two-dimensional grid of Gauss integration points is employed for accurate domain integration.*

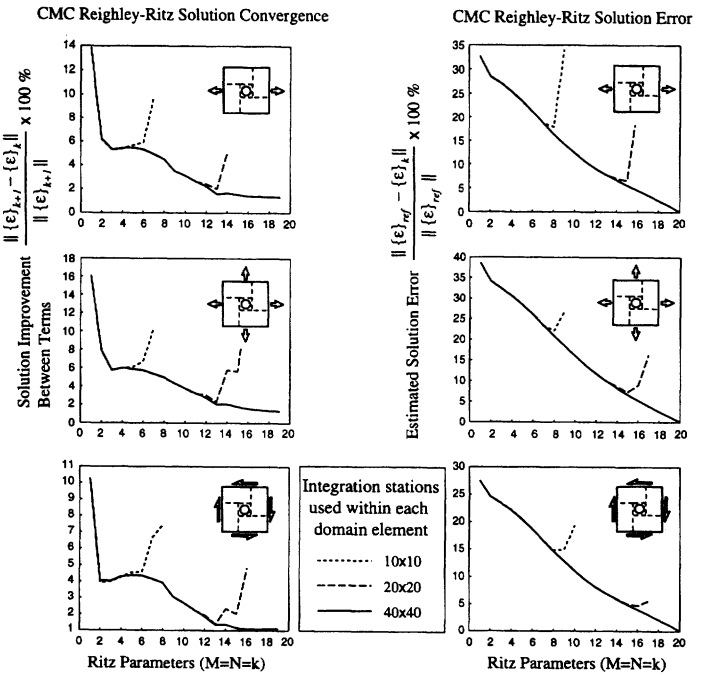

Figure 10. *Left column of plots: Percent difference between consecutive Rayleigh-Ritz solutions as a function of the number of terms used in the series solution. Right column of plots: An estimated error norm of the kth solution relative to a reference solution obtained for M = N = k = 20 using a 40 × 40 grid of Gauss integration points for each domain element shown in Figure 9. Material and geometry data used for a* stiff-ceramic matrix plain weave fabric composite *are those given in Table 3.*

5. CONCLUSIONS

A semi-analytical method capable of predicting the elastic micro-stress fields in *soft*-polymer and *stiff*-ceramic matrix plain weave fabric composites has been developed. The method employs robust unit-cell surface functions developed in Reference [42] as a means of obtaining the spatially varying laminate stiffnesses of elemental columns within the woven unit-cell. The elastic deformations of a 2-D woven plate have been approximated with the aid of the Kirchhoff-Love deformation hypothesis. This semi-analytical Rayleigh-Ritz approximate method also employs a variational form of the elastic potential energy to extract optimal series solutions for the spatially varying mid-plane deformations.

Relevant convergence and error estimate results have been presented for uniaxial, biaxial and pure shear in-plane loading. Convergence and accuracy characteristics have been explored. The reported results have been used to establish guidelines for the optimal selection of series terms for both *soft*-polymer and

stiff-ceramic matrix plain weave composites. Robust integration schemes have been considered and their effects on the solution convergence has been reported. Extensive results comparing the micro-fields and effective properties predicted by the Rayleigh-Ritz method with results obtained by the finite element method and modified lamination theory are presented elsewhere [46,47].

ACKNOWLEDGMENT

Support for this work was provided by the National Science Foundation, Grant No. CMS94-96209.

APPENDIX—NON-DIMENSIONALIZATION

The solutions of the boundary value problems presented in this paper may be scaled with respect to characteristic dimensions such that the solution of one problem will yield results for all self similar problems. The three independent dimensions that are chosen in order to scale the problems are

$$\begin{aligned} L_c &\equiv \text{Characteristic Length} \\ u_c &\equiv \text{Characteristic Displacement} \\ E_c &\equiv \text{Characteristic Modulus} \end{aligned} \tag{A1}$$

All the variables associated with the boundary value problems may be non-dimensionalized with the aid of these three characteristic dimensions. For a given variable, the notation (^) is used to denote the respective variable as dimensionless. The fundamental data related to the characteristic dimensions are the spatial variables x, y and z, the displacement fields u, v, and w, and the local material stiffnesses $\bar{Q}_{ij}$ which are written in the non-dimensional form

$$\begin{aligned} \{x\ y\ z\} &= \{\hat{x}\ \hat{y}\ \hat{z}\}L_c \\ \{u\ v\ w\} &= \{\hat{u}\ \hat{v}\ \hat{w}\}u_c \\ [\bar{Q}_{ij}] &= [\hat{\bar{Q}}_{ij}]E_c \end{aligned} \tag{A2}$$

The two-dimensional stresses and strains at a point in the body take the non-dimensional form

$$\{\varepsilon_x\ \varepsilon_y\ \varepsilon_{xy}\} = \{\hat{\varepsilon}_x\ \hat{\varepsilon}_y\ \hat{\gamma}_{xy}\}u_c/L_c$$
$$\{\sigma_x\ \sigma_y\ \tau_{xy}\} = \{\hat{\sigma}_x\ \hat{\sigma}_y\ \hat{\tau}_{xy}\}E_c u_c/L_c \tag{A3}$$

and the field variables associated with the plate elasticity problem may be non-dimensionalized as

$$\{u_0\ v_0\ w_0\} = \{\hat{u}_0\ \hat{v}_0\ \hat{w}_0\}u_c$$
$$\{\varepsilon_x^0\ \varepsilon_y^0\ \gamma_{xy}^0\} = \{\hat{\varepsilon}_x^0\ \hat{\varepsilon}_y^0\ \hat{\gamma}_{xy}^0\}u_c/L_c$$
$$\{\kappa_x^0\ \kappa_y^0\ \kappa_{xy}^0\} = \{\hat{\kappa}_x^0\ \hat{\kappa}_y^0\ \hat{\kappa}_{xy}^0\}u_c/L_c^2 \tag{A4}$$
$$\{N_x\ N_y\ N_{xy}\} = \{\hat{N}_x\ \hat{N}_y\ \hat{N}_{xy}\}E_c u_c$$
$$\{M_x\ M_y\ M_{xy}\} = \{\hat{M}_x\ \hat{M}_y\ \hat{M}_{xy}\}E_c u_c L_c$$

Consequently, the dimensionless composite plate stiffnesses $\hat{A}_{ij}$, $\hat{B}_{ij}$, and $\hat{D}_{ij}$ are defined by

$$[A_{ij}] = [\hat{A}_{ij}]E_c L_c \qquad [B_{ij}] = [\hat{B}_{ij}]E_c L_c^2 \qquad [D_{ij}] = [\hat{D}_{ij}]E_c L_c^3 \tag{A5}$$

The woven unit-cell geometry parameters are normalized with respect to the characteristic length L_c yielding the non-dimensional parameters

$$a = \hat{a}L_c \qquad b = \hat{b}L_c \qquad g = \hat{g}L_c \qquad l = \hat{l}L_c \qquad h = \hat{h}L_c \qquad t = \hat{t}L_c \tag{A6}$$

In a similar manner the geometry surface functions associated with layer k are normalized with the characteristic length L_c and are

$$s_k = \hat{s}_k L_c \tag{A7}$$

For the effective tow material properties, the Poisson's ratios are dimensionless quantities, and the non-dimensional Young's and shear moduli are related to the dimensional quantities by

$$E_1 = \hat{E}_1 E_c \qquad E_2 = \hat{E}_2 E_c \qquad G_{12} = \hat{G}_{12} E_c \qquad G_{23} = \hat{G}_{23} E_c \tag{A8}$$

and in a similar manner the non-dimensional Young's modulus of the effective matrix is normalized by the characteristic modulus E_c as

$$E_{\hat{m}} = \hat{E}_{\hat{m}} E_c \tag{A9}$$

In the case of the applied displacement boundary conditions, the relationships in terms of the characteristic displacement u_c are

$$u_x^\infty = \hat{u}_x^\infty u_c \qquad u_y^\infty = \hat{u}_y^\infty u_c \qquad u_{xy}^\infty = \hat{u}_{xy}^\infty u_c \tag{10}$$

Subsequently, the non-dimensional Ritz coefficients from the finite series solutions may also be defined by

$$a_{mn} = \hat{a}_{mn} u_c \qquad b_{mn} = \hat{b}_{mn} u_c \qquad c_{mn} = \hat{c}_{mn} u_c \tag{A11}$$

The equations presented in the boundary value problem formulation of section 2 may be written in a non-dimensional form by appropriate substitution of the relationships presented in this appendix. Solution of the non-dimensional boundary value problems will yield results that may be scaled with the quantities L_c, u_c, and E_c consistent with the above equations. For the woven unit-cell problems the characteristic length L_c is set equal to the unit-cell tow undulation half period a, and the characteristic modulus E_c is chosen to be the tow longitudinal modulus E_1. A different characteristic displacement u_c is selected depending on the boundary value problem being solved. For the biaxial and uniaxial displacement problems, $u_c = u_x^\infty$, and for the simple shear problem, $u_c = u_{xy}^\infty$.

REFERENCES

1. Takashi Ishikawa and Tsu-Wei Chou. 1982. "Elastic Behavior of Woven Hybrid Composites," *J. Composite Mater.*, 16:2–19.
2. T. Ishikawa and T. W. Chou. 1982. "Stiffness and Strength Behaviour of Woven Fabric Composites," *J. Mater. Sci.*, 17:3211–3220.
3. Takashi Ishikawa and Tsu-Wei Chou. 1983. "In-Plane Thermal Expansion and Thermal Bending Coefficients of Fabric Composites," *J. Composite Mater.*, 17:92–104.
4. Takashi Ishikawa and Tsu-Wei Chou. 1983. "One-Dimensional Micromechanical Analysis of Woven Fabric Composites," *AIAA J.*, 21(12):1714–1721.
5. Tsu-Wei Chou and Takashi Ishikawa. 1989. "Analysis and Modeling of Two-Dimensional Fabric Composites," In Tsu-Wei Chou and Frank K. Ko, editors, *Textile Structural Composites: Composite Materials Series,* Elsevier Science Publishers B. V., 3:209–264.
6. N. K. Naik and P. S. Shembekar. 1992. "Elastic Behavior of Woven Fabric Composites: I-Lamina Analysis," *J. Composite Mater.*, 26(15):2196–2225.
7. N. K. Naik and V. K. Ganesh. 1992. "Prediction of On-Axes Elastic Properties of Plain Weave Fabric Composite," *Composites Sci. & Tech.*, 45:135–152.

8. K. Ranji Vaidyanathan, Ajit D. Kelkar, and Jagannathan Sankar. 1993. "Prediction of Elastic Properties of Ceramic Matrix Composites Using a Plain Weave Classical Laminate Theory," *Ceram. Engr. Sci. Proc.*, 14(9–10):1066–1076.
9. Ivatury S. Raju and John T. Wang. 1994. "Classical Laminate Theory Models for Woven Fabric Composites," *J. Composite Tech. & Res.*, 16(4):289–303.
10. Wen-Shyong Kuo and Tsu-Wei Chou. 1995. "Elastic Response and Effect of Transverse Cracking in Woven Fabric Brittle Matrix Composites," *J. Amer. Ceram. Soc.*, 78(3):783–792.
11. N. K. Naik and V. K. Ganesh. 1996. "Failure Behavior of Plain Weave Fabric Laminates under On-Axis Uniaxial Tensile Loading: II–Analytical Predictions," *J. Composite Mater.*, 30(16):1779–1822.
12. Y. C. Zhang and J. Harding. 1990. "A Numerical Micromechanics Analysis of the Mechanical Properties of a Plain Weave Composite," *Computers and Structures*, 36(5):839–844.
13. John D. Whitcomb. 1991. "Three-Dimensional Stress Analysis of Plain Weave Composites," In T. K. O'Brien, editor, *Composite Materials: Fatigue and Fracture (Third Volume)*, ASTM STP 1110, American Society for Testing and Materials, Philadelphia, pp. 417–438.
14. A. Dasgupta and S. M. Bhandarkar. 1994. "Effective Thermomechanical Behavior of Plain-Weave Fabric-Reinforced Composites Using Homogenization Theory," *Engr. Mater. & Tech.*, 116:99–105.
15. S. Shkoller and G. Hegemier. 1995. "Homogenization of Plain Weave Composites Usnig Two-Scale Convergence," *I. J. Sol. & Struc.*, 32(6–7):783–794.
16. R. A. Naik. 1994. "Analysis of Woven and Braided Fabric Reinforced Composites," *NASA Contractor Report 194930.*
17. Brian N. Cox. 1995. "Failure Models for Textile Composites," *NASA Contractor Report 4686.*
18. R. A. Naik. 1996. "Analysis of Woven and Braided Fabric Reinforced Composites," In R. B. Deo and C. R. Saff, editors, *Composite Materials: Testing and Design (Twelfth Volume), ASTM STP 1274*, American Society for Testing and Materials, pp. 239–263.
19. Brian N. Cox and Gerry Flanagan. 1997. "Handbook of Analytical Methods for Textile Composites," *NASA Contractor Report 4750.*
20. Robert M. Jones. 1975. *Mechanics of Composite Materials.* Hemisphere Publishing Corp.
21. Takashi Ishikawa, Masamichi Matsushima, Youichi Hayashi and Tsu-Wei Chou. 1985. "Experimental Confirmation of the Theory of Elastic Moduli of Fabric Composites," *J. Composite Mater.*, 19:443–458.
22. Z. Hashin. 1983. "Analysis of Composite Materials—A Survey," *J. Appl. Mech.*, 50:481–505.
23. J. L. Kuhn and P. G. Charalambides. 1998. "Elastic Response of Porous Matrix Plain Weave Fabric Composites: Part I—Modeling," *J. Composite Mater.*, 32(16):1426–1471.
24. J. L. Kuhn and P. G. Charalambides. 1998. "Elastic Response of Porous Matrix Plain Weave Fabric Composites: Part II—Results," *J. Composite Mater.*, 32(16):1472–1507.
25. Jacob Aboudi. 1989. "Micromechanical Analysis of Composite by the Method of Cells," *Appl. Mech. Rev.*, 42(7):193–221.
26. R. M. Christensen. 1979. *Mechanics of Composite Materials*, John Wiley and Sons, Inc.
27. J. N. Reddy. 1984. *Energy and Variational Methods in Applied Mechanics*, John Wiley and Sons, Inc.
28. C. Cinquini, C. Mariani and P. Venini. 1995. "Rayleigh-Ritz Analysis of Elastically Constrained Thin Laminated Plates on Winkler Inhomogeneous Foundation," *Comp. Meth. Appl. Mech. Engr.*, 123:263–286.
29. K. M. Liew and C. M. Wang. 1993. "pb-2 Rayleigh-Ritz Method for General Plate Analysis," *Eng. Struct.*, 15(1):55–60.
30. R. L. Yuan and L. S. Wang. 1991. "Generalized Variational Principle of Plates on Elastic Foundation," *J. Appl. Mech.*, 58:1001–1004.
31. M. Savoia, F. Laudiero and A. Tralli. 1994. "A Two-Dimensional Theory for the Analysis of Laminated Plates," *Comp. Mech.*, 14:38–51.

32. V. G. Piskunov, V. E. Verijenko, S. Adali and E. B. Summers. 1993. "A Higher-Order Theory for the Analysis of Laminated Plates and Shells with Shear and Normal Deformation," *Int. J. Engng. Sci.*, 31(6):967–988.
33. Yibin Fu and Zhenghua Li. 1993. "An Asymptotic Stress Analysis of Laminated Plates," *I. J. Sol. & Struc.*, 30(23):3245–3260.
34. Sun Liangxin and Shi Zhyu. 1992. "The Analysis of Laminated Composite Plates Based on the Simple Higher-Order Theory," *Computers and Structures*, 43(5):831–837.
35. P. Gaudenzi. 1992. "A General Formulation of Higher-Order Theories for the Analysis of Laminated Plates," *Composite Structures*, 20:103–112.
36. J. N. Reddy. 1990. "On Refined Theories of Composite Laminates," *Meccanica*, 25:230–238.
37. E. J. Barbero, J. N. Reddy and Jan Teply. 1990. "An Accurate Determination of Stresses in Thick Laminates Using a Generalized Plate Theory," *Int. J. Num. Meth. Engr.*, 29:1–14.
38. J. N. Reddy. 1987. "A Generalization of Two-Dimensional Theories of Laminated Composite Plates," *Comm. App. Num. Meth.*, 3:173–180.
39. J. N. Reddy. 1984. "A Simple Higher-Order Theory for Laminated Composite Plates," *J. Appl. Mech.*, 51:745–752.
40. J. M. Whitney and N. J. Pagano. 1970. "Shear Deformation in Heterogeneous Anisotropic Plates," *J. Appl. Mech.*, pp. 1031–1036.
41. N. J. Pagano. 1970. "Exact Solutions for Rectangular Bidirectional Composites and Sandwich Plates," *J. Composite Mater.*, 4:20–34.
42. J. L. Kuhn and P. G. Charalambides. 1998. "Modeling of Plain Weave Fabric Composite Geomtry," Submitted to *J. Composite Mater.*, in press.
43. S. G. Lekhnitskii. 1963. *Theory of Elasticity of an Anisotropic Elastic Body*, Holden-Day, Inc. Translated by P. Fern; edited by Julius J. Brandstatter.
44. Jonathan L. Kuhn. 1997. *Mechanical Behavior of Woven Ceramic Matrix Composites*, PhD. thesis, The University of Maryland, Baltimore County.
45. J. L. Kuhn and P. G. Charalambides. 1997. "On the Accuracy of Approximate Elastic Microfields in Plain Weave Fabric Composites Under In-Plane Loading," Submitted to *J. Composite Mater.*, November.
46. J. L. Kuhn and P. G. Charalambides. "Elastic Micro-Fields and Effective Properties of Polymer Matrix Plain Weave Fabric Composites," in progress.
47. S. I. Haan, J. L. Kuhn and P. G. Charalambides. 1997. "Elastic Response of Plain Weave Ceramic Matrix Composites Under Remote In-Plane Loading," submitted to *J. Amer. Ceram. Soc.*, November.